PEOPLE'S DEMOCRATIC REPUBLIC OF ALGERIA

MINISTRY OF HIGHER EDUCATION AND SCIENTIFIC RESEARCH

UNIVERSITY OF MEDEA

FACULTY OF SCIENCES



MASTER OF SCIENCE

In Physics

Discipline: Theoretical Physics

By:
KADIK ABDERRAHMANE

Theme:

Study and characterization of a photodiode for radiation measurement

Publicly defended, on 06/27/2022, before the jury composed of:

HOUATIS Djamel	MCA	U. MEDEA	President
RADJEAI Missoum	MCA	U. MEDEA	Examiner
BOURENANE Aissa	Specialized engineer	CRNB, Ain-Oussera	Examiner
BELARAGUEB Chaabane	Research associate	CRNB, Ain-Oussera	Supervisor
ZITOUNI Hannachi	Pr	U. MEDEA	Co-supervisor

Academic year 2021-2022

Dedications

To my parents.

Acknowledgement

First of all, thank to Allah and to all those who have helped me throughout our education from primary school to the last days at university. The work presented in this master's thesis is the result of close collaboration with our supervisor M.CHAABANE Belarageb who was both my colleague and my supervisor. I thank him with particular recognition for the exceptional quality of his training, his unconditional support and his always enlightened advice. I am thankful to my second supervisor Prof. Zitouni Hannachi, whose guidance helped me to mature from a scientific point of view. Thanks a lot to his continuous encouragement, technical guidance and psychological support for more than three years. I'm also thankful to M. BOURENANE Aissa who always help me and push me to achieve high-performance as a top-quality scientific worker in MCNP, Thanks to BOUKERDJA Ayachi for his suggestions and discussions during my research. And Thank to Mme. Kasida Naggara to provide us her laboratory and help .

We would like to thank those who accepted to be members of the jury for the defense of our master's thesis, the president Dr. HOUATIS Djamel, Doctors RADJEAI Missoum, who accepted to examine our work. We would also like to thank all our teachers who participated in our training throughout the university course.

I am particularly thankful to my parents for their continuous support in every moment of my life, right from the childhood to date. For everything you did, for all the suggestions, prayers and love. You are special to me! I am thankful to my siblings, for their exceptional love, help and support throughout my life, special thanks for psychologically supporting me in the hard moments when everything seemed so difficult to me.

My experience at CRNB has been an unprecedented and unique period of my life. I had the luck and honor to work with and benefit from some extraordinary people. Expressing my gratitude to all those people in a single page feels impossible I still hold so much pride and respect for them.

ملخص

يعتبر هذا العمل مساهمة في تطوير جهاز قياس الإشعاعات لمخبر الإلكترونيك النووي لمركز الابحاث النووية. فلأول مرة ننجح في استعمال جهاز كشف أشباه الموصلات الجديد وهو " PIN photodiode " . يستخدم الثنائي الضوئي PIN مؤخرًا (مناسب أصلاً للكشف عن الضوء) ككاشفات إشعاع في تطبيقات مختلفة مثل التحليل الطيفي لأشعة X وأشعة جاما (كفاءة 100 ٪ حتى 10 كيلو فولت)، والجسيمات المشحونة (حتى 12 ميغا إلكترون فولت) لتحديد المواد المشعة. بالإضافة إلى ذلك ، يتم استخدامه في مراقبة الفوتون في آلات الأشعة السينية في التطبيقات الصناعية والطبية وأيضًا في مراقبة شدة الفوتون في المسرع (حتى 18 ميجا فولت) وحول محطة الطاقة النووية.

التكلفة المنخفضة للديود الضوئي للسيليكون، ووفرتة، ودقته في تحديد الموضع نظرًا لصغر حجمه وحساسيته الجيدة لمجالات الإشعاع المختلفة، حفزنا على تطوير الدائرة الإلكترونية المرتبطة بكاشف أشباه الموصلات هذا، للسماح باستخدامه في تطبيقات تخص مجالات مختلفة. كخطوة أولى خلال هذه العمل، ركزنا على دراسة وتوصيف الثنائي الضوئي "OPF430 PIN " . تم الحصول على طيف جيد لأشعة ألفا مقارنة بالكاشف (SSB). لم نحصل على أطياف جيدة لأشعة جاما والأشعة السينية بسبب ضعف اشارة الكاشف للطاقة المنخفضة اضافة إلى الحساسية المحدودة للمضخم الأولي.

على الرغم من ذلك، تحصلنا على كفاءة جيدة لنتائج محاكاة أشعة جاما باستخدام تطبيق "MCNP5 " من خلال بناء النموذج الخاص بنا والذي يتلاءم جيدًا مع البيانات التجريبية المنشورة في مقالات عالمية مختلفة.

الكلمات المفتاحية (كاشف نووي والإشعاعي، ديودات PIN ، أشعة إكس، أشعة جاما وألفا، التحليل الطيفي).

Abstract

This work is a contribution to the instrument radiation measurement for the nuclear electronic laboratory of the center by the introduction, for the first time, through this work of a new semiconductor detector, which is the PIN photodiode.

Recently PIN photodiode (originally suited for light detection) are used as radiation detectors in various applications such spectroscopy of X and gamma rays (100% efficiency up to 10 keV), and charged particles (up to 12 MeV) for the identification of radioactive materials. In addition, it is used in photon monitoring in X ray machines in industrial and medical applications and also in the monitoring of intensity of photon in accelerator (up to 18 MeV) and around of nuclear power plant.

The low cost of silicon PIN photodiode, its abundance, its good position resolution due to its small size and its good sensitivity for different radiation fields, motivate us to develop the electronic circuit associated with this semiconductor detector in order to permit its use in different application area.

As a first step through this dissertation, we have focused on the study and characterization of the OPF430 PIN photodiode. A good alpha spectrum was obtained compared to the SSB (Silicon Surface Barrier) detector. We have not obtained a good gamma and X ray spectra due to the detector response limited for low energy (10keV) added to the limited used preamplifier sensitivity.

Although, we obtained a good efficiency of gamma ray simulation result using MCNP5 code (through our model construct) which fitted well with experimental data published in different papers.

Keywords (Nuclear Detector, PIN diodes, X-rays, Gamma rays, spectroscopy).

Résumé

Ce travail est une contribution à l'instrument de mesure du rayonnement pour le laboratoire d'électronique nucléaire du centre par l'introduction, pour la première fois, d'un nouveau détecteur à semi-conducteur, qui est la photodiode PIN. Récemment, la photodiode PIN (dediée à l'origine à la détection de la lumière) est utilisée comme détecteur de rayonnement dans diverses applications telles que la spectroscopie des rayons X et gamma (efficacité de 100% jusqu'à 10 keV) et des particules chargées (jusqu'à 12 MeV) pour l'identification de matières radioactives.

En outre, il est utilisé dans la surveillance des photons dans les machines à rayons X dans les applications industrielles et médicales et également dans la surveillance de l'intensité des photons dans les accélérateurs (jusqu'à 18 MeV) et autour des centrales nucléaires. Le faible coût de la photodiode PIN au silicium, son abondance, sa bonne résolution de position due à sa petite taille et sa bonne sensibilité pour différents champs de rayonnement, nous motivent à développer le circuit électronique associé à ce détecteur à semi-conducteur afin de permettre son utilisation dans différents champs d'applications.

Dans une première étape de cette thèse, nous nous sommes concentrés sur l'étude et la caractérisation de la photodiode PIN OPF430. Un bon spectre alpha a été obtenu comparé au spectre du détecteur SSB (Silicon Surface Barrier). Nous n'avons pas obtenu de bons spectres gamma et X en raison de la faible amplitude du signal détecteur pour les basses énergies ajoutées à la sensibilité limitée du préamplificateur utilisé. Cependant, nous avons obtenu une bonne efficacité du résultat de la simulation des rayons gamma et X en utilisant le code MCNP5 (via notre modèle de construction) qui correspondait bien aux données expérimentales publiées dans différents articles.

Mots-clés (Détecteur Nucléaire, Diodes PIN, Rayons X, Rayons Gamma, spectroscopie).

Table of contents

Dedications 2
Acknowledgement 3
ملخص 4
Abstract 5
Résumé 6
Table of contents 7
Abbreviations list 1
List of figures 2
List of Tables 4
Introduction 5
Chapter 1 7
1 Radiation and interaction 7
1.1 Introduction 7
1.2 Radiation Sources 7
1.2.1 Alpha 7
1.2.2 Fast electron 8
1.2.3 Gamma and x-ray 8
1.3 Radiation interaction 8
1.3.1 Interaction of x-ray and gamma ray with matter 8
1.3.1.1 Photoelectric effect 9
1.3.1.2 Compton scattering 9
1.3.1.3 Pair production 10
1.3.1.4 Mass attenuation coefficient 10
1.3.2 Interaction of heavy charged particle 12
1.3.2.1 Stopping power 12
1.3.2.2 Energy straggling and particle range 13
Chapter 2 14
2 Types of detectors 14
2.1 Introduction 14
2.2 Gas field detector 14

2.2.1 Ionization chamber 14
2.2.2 Proportional counters 15
2.2.3 Geiger-Muller counters 16
2.3 Non-gases detectors 17
2.3.1 Scintillation detectors 17
2.3.1.1 Scintillation detectors mechanism 17
2.3.2 Semiconductor detectors 18
2.3.2.1 Introduction 18
2.3.2.2 Semiconductors types 19
2.3.3 Semiconductors as radiation detectors 21
2.3.3.1 PN-Junction 21
2.3.3.2 PIN junction 24
2.3.3.3 Surface barrier detector 25
2.3.3.4 Properties of P_N junctions 26
Chapter 3 29
3 Detector Signal Processing 29
3.1 Electronic associated to detector 29
3.1.1 Preamplifier. 29
3.1.2 Current mode 29
3.1.3 Pulse mode 30
3.1.3.1 Case 1 $\tau = RC \ll tc$ 31
3.1.3.2 Case 2 $\tau = RC \gg tc$ 31
3.1.4 Amplifier: 33
3.1.5 ADC Resolution 33
3.1.6 MCA, ... 33
3.2 Pulse height spectra 34
3.3 Energy resolution 34
3.4 Efficiency 35
Chapter 4 37
4 OPF430 PIN Photodiode Characterization. 37
4.1 Introduction 37
4.2 Experimental banc 38
4.3 Leakage (or Dark) current 39
4.4 Photodiode Capacity 40
4.5 Alpha radiation measurement 40

4.5.1 Experimental Banc 40
4.5.2 Radiation Source. 41
4.5.3 Experimental Protocol 41
4.5.4 Signal Acquisition. 42
4.5.4.1 OPF430 PIN Photodiode Signal Acquisition. 42
4.5.4.2 Barrier surface Signal Acquisition. 42
4.5.4.3 Results discussion 42
4.6 Spectra Acquisition 43
4.6.1 OPF430 PIN Photodiode Spectre Acquisition. 43
4.6.2 Barrier Surface Spectre Acquisition. 44
4.6.3 Result discussion 45
4.7 Spectroscopy of gamma ray at low energy 45
Chapter 5 47
5 Monte Carlo Simulation study 47
5.1 Introduction 47
5.1 MCNP structure and mechanism of working 47
5.1.1 Surfaces 48
5.1.1 Cells card 48
5.1.2 Data specification 49
5.1.2.1 Material specification 49
5.1.2.2 Source of radiation 49
5.1.2.3 Tallies 51
5.2 Construction of OPF 430 pin diode by MCNP5 51
5.2.1 Penetration of radiation 52
5.2.1.1 Attenuation of x ray in glass 52
5.2.1.2 Attenuation of x-ray in paper 53
5.2.1.3 Attenuation of alpha particle in paper 54
5.2.2 Efficiency of gamma rays 55
5.2.2.1 Discussion 56
General Conclusion 57
Appendix: 58

Abbreviations list

FWHM	Full width at half maximum
G-M	Geiger Muller
PC	proportional counter
SSB	silicone surface barrier detector
EGS	Electron Gamma Shower
ITQ	Integrated TIGER Series
MORSE	Multi group Oak Ridge Stochastic Experiment
MCNP	Monte Carlo N particle
SRIM	the Stopping and Range of Electrons in Matter
TRIPOLI	TRIdimensiol POLykinetic
MCA	Multi-Channel Analyser
FEPE	full energy peak efficiency
PIN	p-type Intrinsic an n-type semiconductor

List of figures

Figure 1: Radiation power penetration for different radiation types[1] 7
Figure 2: Energy of electromagnetic radiation. 8
Figure 3: Photoelectric effect [3]. 9
Figure 4: Schematic of the mechanism of Compton scattering [4]. 10
Figure 5: Pair production mechanism[5]. 10
Figure 6: Mass attenuation coefficient. 11
Figure 7 : Attenuation of X ray in Silicon. 12
Figure 8: The specific energy loss along an alpha track [7] 13
Figure 9: Measurement of energy struggling. 13
Figure 10: Gases detectors with different voltage applied in pulse mode. 14
Figure 11: Basic component of an ion chamber and the voltage-current characteristics. 15
Figure 12: Principle of multiplication. 16
Figure 13: Scintillation detectors [7]. 17
Figure 14: Energy band structure of an inorganic scintillator. 18
Figure 15: Different between conductors, semiconductors and insulators [9]. 18
Figure 16: Representation of a donor impurity (phosphorus) occupying a substitutional site in a silicon crystal. (b) Corresponding donor levels created in the silicon band gap [8] 20
Figure 17: Representation of an acceptor impurity (boron) occupying a substitional site in a silicon crystal .(b) corresponding acceptor levels created in the silicon band gap [8]. 21
Figure 18: Combination of P and N type semiconductor 22
Figure 19: Diagram of energy of PN junction before and after the equilibrium. 22
Figure 20: behavior of PN junction +HV[6] 23
Figure 21: Forward baised mode. 23
Figure 22: Reverse biased. 24
Figure 23: Energy band diagram [10] 24
Figure 24: Basic structure of PIN photodiode[11]. 25
Figure 25: Connections of PIN diode with a preamplifier to operate in: a) photovoltaic mode, b) photoconductive mode. 25
Figure 26 Surface Barrier Detector (photo prise au labo). 26
Figure 27 : Rise time. 27
Figure 28 : General Detector chain configuration[12]. 29
Figure 29 The measure of average current 30
Figure 30 Equivalent Detector Circuit 30
Figure 31 : Detector current Pulse. 31
Figure 32: (a) The assumed current output from detector. (b) The signal voltage V(t) for the case of a small time constant load circuit. (c): The signal voltage V(t) for the case of a large time constant load circuit. 32
Figure 33 : Typical charge preamplifier configuration 32

Figure 34 : Configuration of an amplifier 33
Figure 35: Displaying the differential of height stpectrum[4]. 34
Figure 36: Peak distributions for good and poor energy resolutions [4]. 35
Figure 37: Full Width at Half Maximum (FWHM)[4]. 35
Figure 38: Example of the full-energy peak in a differential pulse height spectrum [4]. 36
Figure 39: OPF430F photodiode ; (a) with package (b) electrical symbol 37
Figure 40 : Support of radiation source. 38
Figure 41: Alpha particle support and vacuum : (a) A general view with the pump vacuum, (b) an inside view of the enclosure with barrier surface detector attached at the center of the cover of the enclosure, (c) PIN photodiode adapted to the barrier surface detector support. 38
Figure 42 : Leakage current measurment circuit. At the right the keitly 617 electrometer. 39
Figure 43 : Leakage current 40
Figure 44: The used detection chain. The MCA and the oscilloscope are not visualized**.** 40
Figure 45: Am-241-Pu-239 Radiation source 41
Figure 46 : Rise time at the preamplifier output : (a) without voltage biasing; (b) with voltage biasing. 42
Figure 47 : Rise time at the preamplifier output : (a) Without voltage biasing (b) With voltage biasing,. 42
Figure 48 Am241- Pu239 Alpha spectra with OPF 430 photodiode 43
Figure 49 : OPF430 PIN Photodiode (zoomed) spectre with and without biased voltage. The tail in the non polarized spectre is due to the trap effect [6]. 43
Figure 50 : Am241-PU239 alpha spectra with SSB 44
Figure 51 : PIN photodiode spectrum displayed by MCA firmeware with spectrum features. 44
Figure 52 : Gamma signal at the preamplifier output (upper) and the corresponding amplifier output (down). The signal need more preamplification to be useful. 46
Figure 53 : Low energy gamma rays spectra acquired by OPF430 PIN photodiode : the noise is dominant. 46
Figure 54: Structure of input file of MCNP [15]. 47
Figure 55: Modeling OPF430 pin diode by solid works (*Photo taken on site and modeled by solidworks*). 51
Figure 56: model OPF340 PIN diode in MCNP 5 where (a) is is the top of detector(x y) and (b) is side of the detector (x z) axis (*Photo taken on site and modeled by solidworks*).....52
Figure 57: Penetration of gamma rays in the glass of the PIN diode.....53
Figure 58: Penetration of gamma rays in the window of the PIN diode.....54
Figure 59: Path of alpha particles in the paper. 54
Figure 60: Simulate efficiency of gamma rays.....56
Figure 61: Simulate efficiency of gamma rays [14].....56

List of Tables

Table 1: Properties of Intrinsic Silicon and Germanium [8]. 19
Table 2 : Electrical charactiristic 37
Table 3 : Revers biased VS leakage current.....39
Table 4: Energy liberated by AM-241 and Pu-239.....41
Table 5 : Relation between channel and energy 45
Table 6 resolution for both spectrum(with and without HV).....45
Table 7: MCNP Surface Cards[13].....48
Table 8: Source variables for the SDEF command. 50
Table 9: Types of tallies available in MCNP. The type of particle tallied is denoted by pl [9].....51
Table 10: Efficiency of gamma rays 52
Table 11: Penetration of x-ray in paper. 53
Table 12 : Stopping power.....54
Table 13: Efficiency of gamma rays 55

`

Introduction

Nowadays, radiation and its detection have a wide range of applications, including the treatment of the deadliest diseases such as cancer, the generation of energy, the research of the universe's origins, and the treatment of our food for health. The application and development of radiation technology has increased as a result of most of these breakthroughs, and new applications are continually being created. The value of this advancement in radiation detection technology to society and the economy cannot be overstated. Radiation detectors aid in the detection of disease within the body via medical radiation imaging, the monitoring of nuclear power plants and to ensure no radiation leakage into the environment, and airport cargo screening to ensure passenger safety when planes are free of radiation.

Detectors are commonly employed in the science of spectroscopy for the detection, identification, and quantification of radioactive compounds. In addition, the performance of ionizing radiation within the detector is biased in all detectors. One of the most crucial differences between detectors is the band gap of the material employed in the detector, which affects how much energy is deposited in terms of resolution and efficiency. The performance gap between scintillation and germanium detectors has piqued the curiosity of researchers in a new type of detector known as a silicon semiconductor detector.

The study of the PIN diode as a detector has been the subject of this thesis. The efficiency and use of this gamma ray detector, as well as charged particle spectroscopy, have been covered in the creation of this work. We also checked the correctness of our work using the Monte Carlo n particle software. This work has divided into three area, the first topic we was discussed broadly the radiation and their interaction with material medium of detectors, the second area cover different type of detectors and how they work, the third area of interest in our research was the use of PIN as a detector for x-ray spectroscopy and charged particles, particularly alpha particles. We compared our results to those obtained using other detectors, such as a surface barrier detector, which is a PN junction with a larger active area than the PIN diode, allowing us to clearly see the phenomena that occurred in the PIN diode. At the end of this section, we build an OPF 430 pin diode with MCNP5 and compute the efficiency with the help of, especially for gamma rays at low energies, because the energy of incoming photons has a considerable effect on the experience.

This research work was carried out within the framework of a collaboration between the department of materials sciences and the nuclear research center of Birine (CRNB). We

mention that the CRNB provided us with all the material and human resources to carry out our internship.

This work gathered between simulation and experiment to study PIN diode, so it becomes for the first time as a detector in CRNB thanks to Allah give us the energy to end this work, on 13-04-2022 the first spectra of alpha particles obtained by this kind of detector few days later we obtain a gamma rays spectra.

Chapter 1

1 Radiation and interaction

1.1 Introduction

Radiation is a form of energy that appears as waves or particles, which split into two different categories charged and uncharged radiation. Both of them called ionizing radiation except of some case such as neutron, which is an indirect ionizing particle because of their neutral charge. Their energy range spans from 10 eV to 20 MeV. There are also some classes of electromagnetic radiation like microwave, radio radiation… etc. That called non ionizing radiation because of their low energy ionization.

Charged radiation include beta particle (positive or negative), alpha particle and fragments fission. Uncharged particle include electromagnetic radiation specially x-ray and gamma ray. Each radiation above differs to each other by their power of penetration for different material thicknesses as it shown in Figure 1.

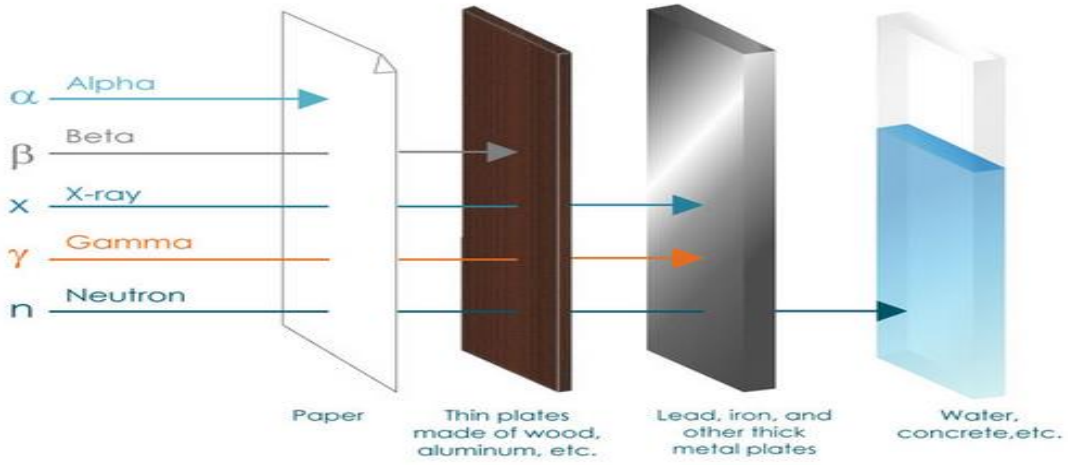


Figure 1: Radiation power penetration for different radiation types[1] .

1.2 Radiation Sources

The radiation source created through many processes, which originate from a nuclear or atomic level. Several types of radiation sources can be given in the following.

1.2.1 Alpha

The most common process to produce alpha are spontaneous fission, accelerator, and alpha decay. The energy of this particle ranged from 4 MeV to 8 MeV and could lose its energy in material very quickly.

1.2.2 Fast electron

It includes beta particles (positives and negative) emitted in nuclear decay and by other process yielding energetic electrons.

1.2.3 Gamma and x-ray

Gamma and x-ray, both of them is an electromagnetic radiation they differ only in the energy, which lead to a different penetration. X rays emitted by a rearrangement of electrons shells of atoms and gamma ray emitted from energy transitions of the nucleus. The energy of X- rays ranged from 100 eV to 10 keV.

Gamma ray are mainly emitted by the excited final nucleus through decay beta or nuclear reaction or in annihilation radiation that occur when positron emitted through beta-pulse decay generally interact with electron and create an electromagnetic radiation. The energy of gamma-rays is great than 10 keV.

The most common way to produce x-ray are excited electron in atom or bremsstrahlung effect which is mainly happened when the fast electron don't interact completely with matter some of the energy transfers to bremsstrahlung [1], usually happened when electron or positron has energy above than a 100 MeV [2].

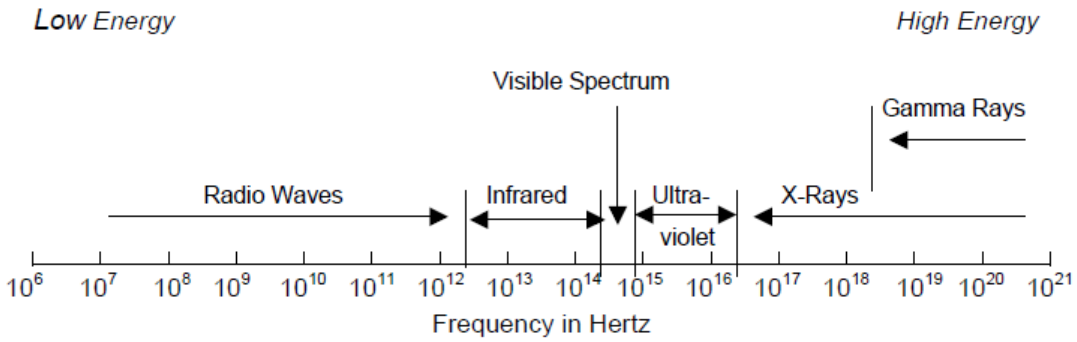


Figure 2: Energy of electromagnetic radiation.

1.3 Radiation interaction

The interaction between radiation and matter is the basis of the detector functioning principle. The understanding of the interaction mechanism of the radiation with the detector medium defines the response of the detector to this radiation.

1.3.1 Interaction of x-ray and gamma ray with matter

Gamma and x-ray have a high-level power penetration because they are uncharged particle, and then there is no loss of their energy via Coulomb force. This kind of radiation interacts with matter through three major interactions: the photoelectric effect, Compton scattering, and pair production.

1.3.1.1 *Photoelectric effect*

Photoelectric absorption mainly happened when incident photon, which has a low energy at approximately less than 0.1 MeV [2], interact with material that has a high atomic number. A part of photon energy is spent to free electron and the rest is converted into its kinetic energy. The probability of this interaction described mathematically by Bragg & Pierce relation as:

$$\tau = const * \frac{Z^n}{E_\gamma^{3.5}}, \qquad 1.1$$

which produce a free photo-electron (electron excited by incoming photon) as you can see in Figure 3.

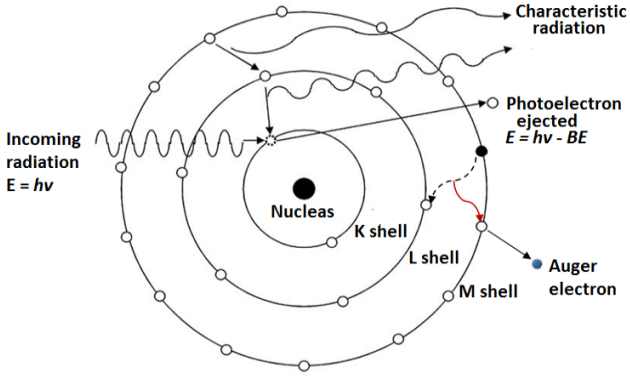


Figure 3: Photoelectric effect [3].

1.3.1.2 *Compton scattering*

When the photon enters with energy ranged from 2.5MeV to 100MeV to the material, the-predominate interaction is Compton scattering, resulted a recoil of both photon and electron because the photon transfers a part of its energy into the electron as it is shown in Figure 4. The probability of Compton scattering is independents to the atomic number of the material, it depends only the path of interaction if there are electrons or not [2] .

The final energy of photon mathematically described as:

$$h\nu' = \frac{h\nu}{1 + \frac{h\nu}{m_0 c^2}(1 - cos\theta)} \qquad 1.2$$

Where $m_0 c^2$ is the mass of electron at rest (0.511 MeV), hν and hν' is the energy of before and after collision of photon respectively.

.

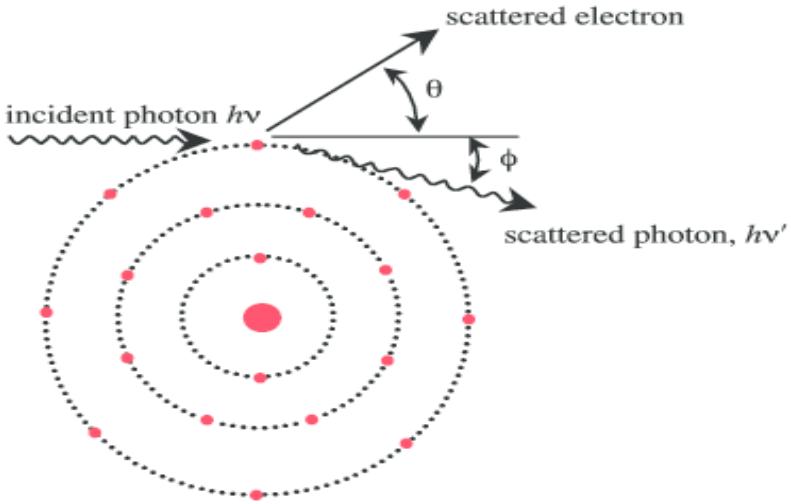


Figure 4: Schematic of the mechanism of Compton scattering [4].

Notice: when energy of incoming photon ranged from 1 MeV to 2.5 MeV both of photoelectric and Compton scattering happened at the same time.

1.3.1.3 *Pair production*

Usually happened when photon has energy more than 1.02 Mev pass through the nucleus lead to the creation of pair ion, in this context means the creation electron and positron (Figure 5).

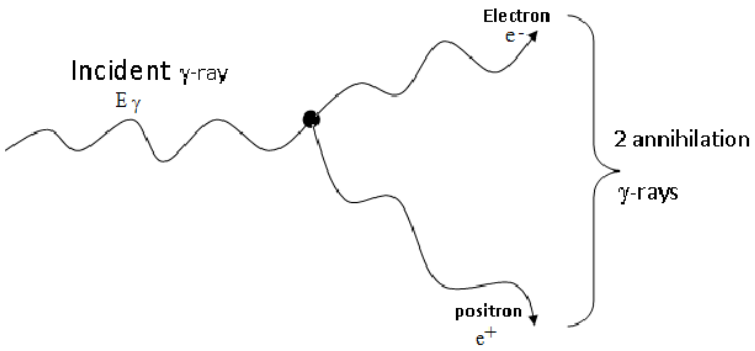


Figure 5: Pair production mechanism[5].

1.3.1.4 *Mass attenuation coefficient.*

The mass attenuation coefficient, or mass narrow beam attenuation coefficient of a material is the attenuation coefficient normalized by the density of the material. The values of mass attenuation coefficients, based on proper values of photon cross section, are dependent upon the absorption and scattering of the incident radiation caused by several different mechanisms such as Rayleigh scattering (coherent scattering); Compton scattering (incoherent scattering); photoelectric absorption; pair production[1].

[1] https://en.wikipedia.org/wiki/Mass_attenuation_coefficient

The number of transmitted photons I is then given in terms of:

$$I = I_0 e^{-\mu x} \quad 1.3$$

Where μ is total linear attenuation coefficient given by:

$$\mu = \tau\ (photoelectric) + \ \sigma(compton) + \pi(pair\ creation) \quad 1.4$$

And total mass attenuation coefficient is given by $\frac{\mu}{\rho}\ (cm^2/g)$. The mass absorption coefficient is then:

$$\frac{\mu_{en}}{\rho} = \frac{\mu}{\rho}(1 - g) \quad 1.5$$

The fraction g represents the energy losses from the materiel.

The mass attenuation coefficient is related to every cross section by:

$$\frac{\mu}{\rho} = \ N_a \ \frac{Z}{A}\ \sigma \quad 1.6$$

Where σ is the total cross-section.

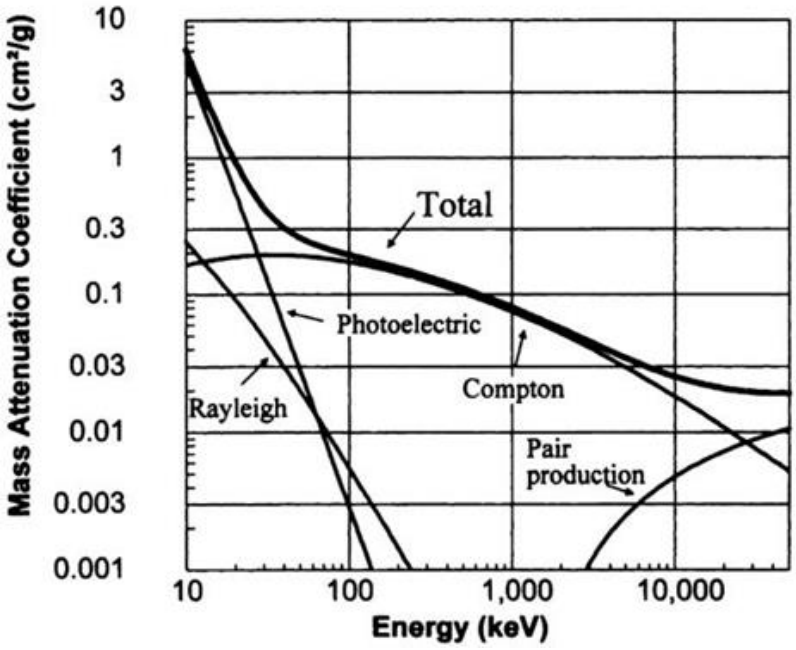


Figure 6: Mass attenuation coefficient[2].

You can see below the absorption of X ray In silicone material in Figure 7.

[2] https://scientificsentence.net/Radiations/index.php?key=yes&Integer=attenuation

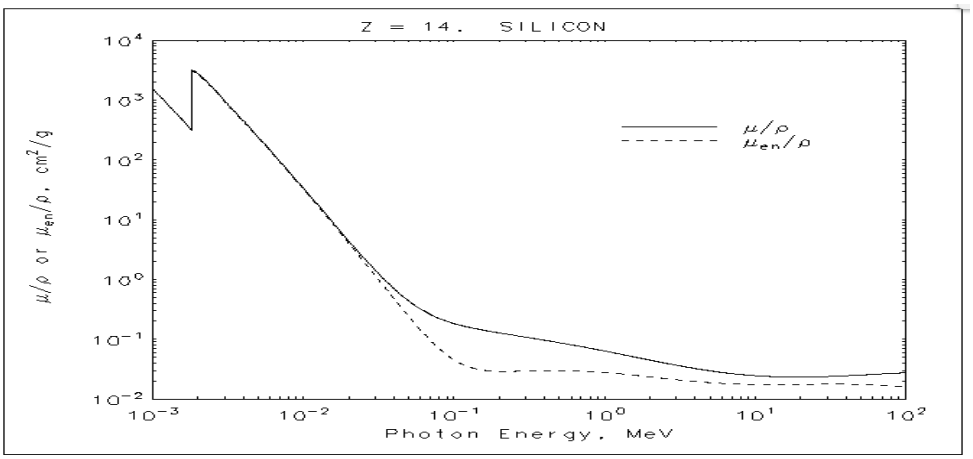


Figure 7 : Attenuation of X ray in Silicon[3].

1.3.2 Interaction of heavy charged particle

It is the case when the Coulomb force is predominant means that the interaction occurs between the charges. The incoming charged particle may excited or ionizing the atom depends only the frequency of the initial charged particle, every single charged particle may interact with several electrons as well as each electron could achieve $\frac{1}{500}$from the energy of initial charged particle [6]. As the charged particle passes the material, several events can occur which can be listed below.

1.3.2.1 *Stopping power*

The loose of energy of the charged particle in the material a described mathematically by the **Bethe** formula [7] as:

$$-\frac{dE}{dx} = \frac{4\pi e^4 z^2}{m_0 v^2} NZ \left[ln\left(\frac{2m_0 v^2}{I}\right) - ln\left(1 - \frac{v^2}{c^2}\right) - \frac{v^2}{c^2} \right] \qquad 1.7$$

Where v and ze are the velocity and charge of incident particle;

N and Z are the number density and atomic number of material absorber;

I is the average excitation and ionization of material absorber.

Notice: Charged particle is non-relativistic $v << c^2$.

It's readily appear from the Figure 8 and Bethe formula when we decrease the velocity of incoming particle lead to the increase of the loss of energy, this technic is widely used in the field of medical.

[3] https://physics.nist.gov/PhysRefData/XrayMassCoef/ElemTab/z14.html

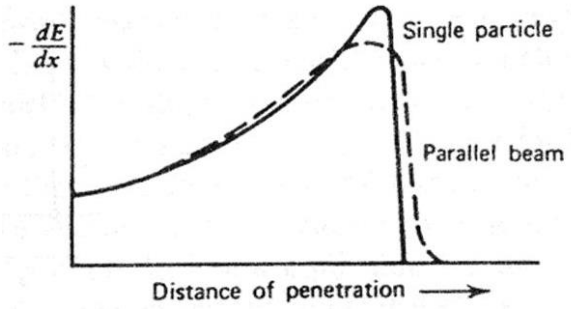


Figure 8: The specific energy loss along an alpha track [7]

1.3.2.2 *Energy straggling and particle range*

Because energy loss is a statistical process, both stopping power and range should be viewed as mean (or average) values over a group of atoms or molecules. It's normal to expect fluctuations. These variations are referred to as straggling in general, and can come in a variety of forms.The most important is range straggling, which implies that particles in the same medium have different journey lengths between the identical initial and ultimate energy due to statistical factors [4].

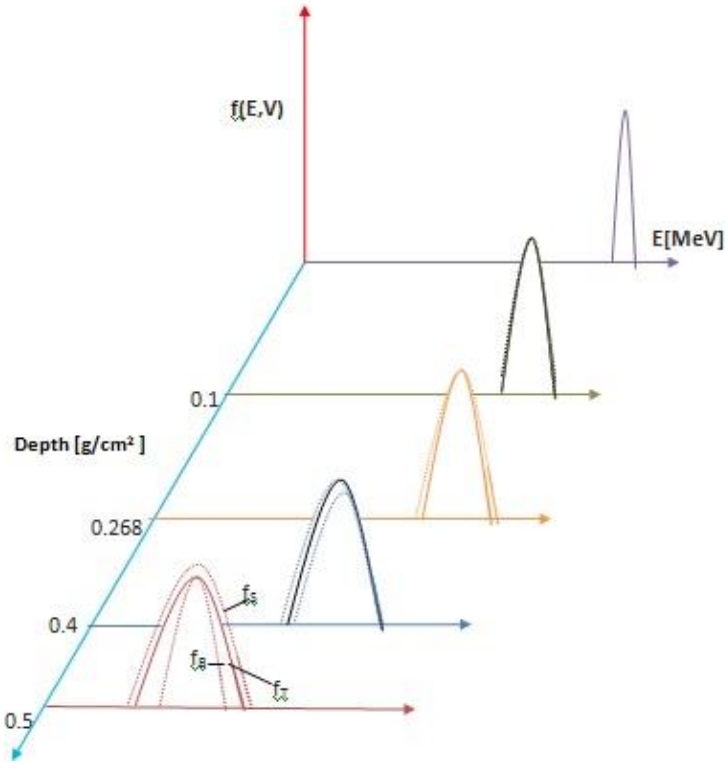


Figure 9: Measurement of energy struggling[5].

[4] https://www.britannica.com/science/radiation/Range
[5] https://commons.wikimedia.org/wiki/File:Energy_Straggling_Effect.jpg

Chapter 2

2 Types of detectors

2.1 Introduction

The detectors classified by their material medium or the region where the interaction happened. There are two great categories gasses and non-gasses detector, each detector use to detect some kind of radiation and differ to other by its efficiency, mode of operation, and energy resolution.

2.2 Gas field detector

The majority of gas-filled detectors are based on sensing the direct ionization created by the passage of the radiation in the gas medium detector. Gas detectors include ionization chamber, proportional counter, and Geiger Muller detector all of them work with the same principle that is the ionization. There are also constructed with the same configuration. The main differences are the mode of operation, the types of gases within detectors, and the voltage applied which is responsible for the distribution and migration of the charge within the detector as it is in Figure 10.

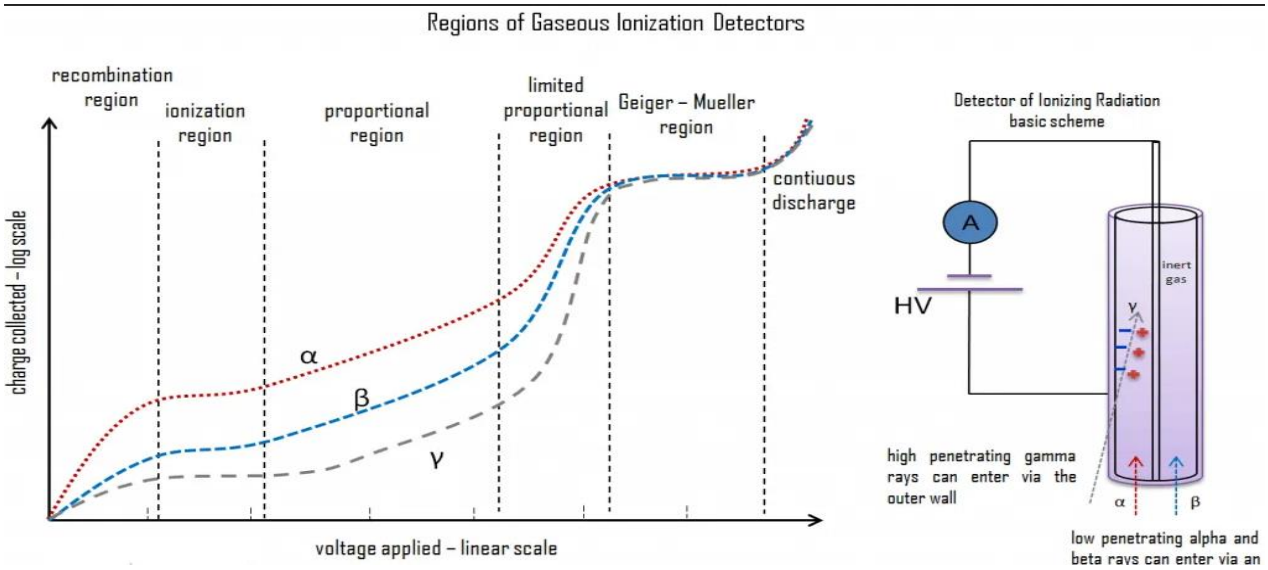


Figure 10: Gases detectors with different voltage applied in pulse mode[6].

2.2.1 Ionization chamber

In the ionization chamber, the charge recombination is negligible due to the low effect of the electric field to the pair holes ion, work only in the principal of ionization also, it works

[6]https://www.radiation-dosimetry.org/fr/quest-ce-que-le-compteur-proportionnel-detecteur-proportionnel-definition/

in both current and pulse mode, that used widely in spectroscopy of x-ray, gamma-ray, and beta radiation.

Ionization and migration process

When charged particle interact with gases then may excited or ionized the molecule that lead to the liberation of both positive ion and free electron. The amount of ion created by incident radiation called (the facto factor) which is affect the energy resolution. This ion pair has accelerated in opposite direction for the reason of the presence of the electric field with velocity equal a:

$$V_d(e) = \frac{\mu_e}{p} E, \qquad 2.1$$

where μ_e is the electron mobility, p is the pression of the medium and E is the electric field.

This drift of this pair ion would create a current know as ionization current as it is in Figure 11.

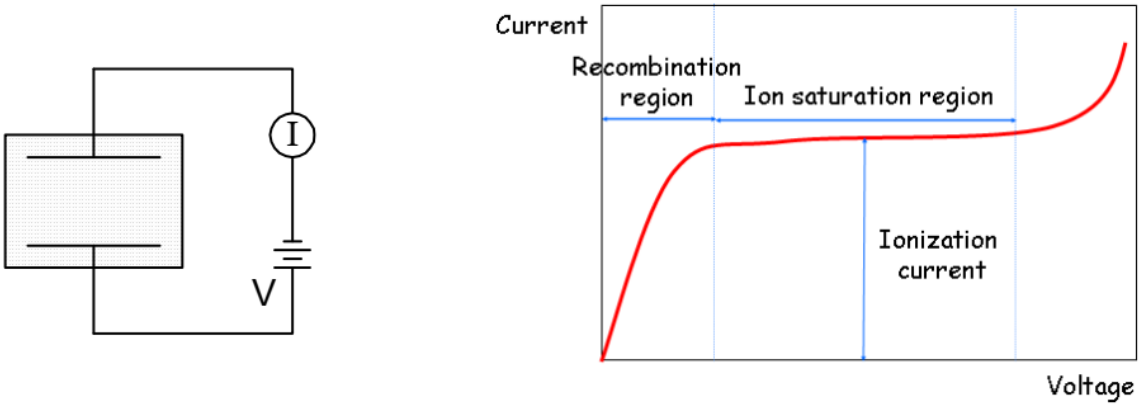


Figure 11: Basic component of an ion chamber and the voltage-current characteristics[7].

2.2.2 Proportional counters

By utilizing gas-filled detectors in a new way, the tiny pulse amplitude encountered in ion chambers can be rectified. The phenomena of gas multiplication is used by a proportional counter to raise the pulse size by hundreds or thousands of times. It detects low-energy radiation in pulse mode, similar to the G-M counter. Depending on the kind of radiation spectroscopy, a rare gas such as Ar, Xe, or K is usually used as a material medium. we represent the variation of the height of the pulse as a function of the applied voltage.

Gas multiplication process

The primary electrons liberated by the incident radiation acquire a sufficient energy for the reason of increasing the eclectic field, lead to a secondary ionization, the electrons

[7] https://science.mcmaster.ca/radgrad/images/6R06CourseResources/4R6Notes3_GasFilled_Detectors.pdf

liberated in secondary ionization accelerated again through the electric field force, this process still happened until they reach the anode known as Townsend avalanche, as it is show in Figure 12.

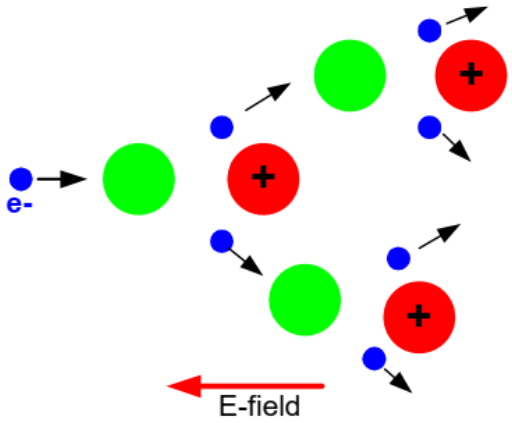


Figure 12: Principle of multiplication[8].

Called proportional counter (PC) is because the total charge produce within detector related to the primary produced by incident radiation by this relation:

$$Q = n_0 eM, \qquad 2.2$$

Where Q is the total charge generated by n_0 pairs and M represent the average gas multiplication .

2.2.3 Geiger-Muller counters

G-M counter work with the same principle with PC the only differences is that the Townsend avalanche that happened in PC by the effect of radiation, heir in G-M counter will occur many times along the entire of the tube of G-M counter. For this amount of electrons reach the anode the detector cannot distinguish between the incident radiations, it just recorded a count, non-matter what the type of incoming radiation.

Each Townsend avalanche may produce at least one photon (UV or visible photon) from bremsstrahlung effect lead to generate another primary electron, which also subjects to another chain reaction know as Townsend avalanche.

Dead time

When radiation enter the detector lead to create a pair ion, and this ion would experience several event like migration, bremsstrahlung effect, Townsend avalanche, and so on until the elections comeback to cathode. During this time G-M counter will not be able to receive any external radiation for that reason called “dead time”.

[8] https://science.mcmaster.ca/radgrad/images/6R06CourseResources/4R6Notes3_GasFilled_Detectors.pdf

In addition, as any detector need some time to return to its normal state to be able to counting a secondary discharge or a period of stabilization of both electric field and distribution of pair ion in the detector, sometimes called resolution time.

2.3 Non-gases detectors

2.3.1 Scintillation detectors

One of the most important ionizing radiation detection techniques. It uses a scintillator as the detector's material support; this sort of substance might be solid, liquid, or gaseous. The notion of incident radiation excitation effect is used to transform incoming radiation such as beta particles, alpha particles, gamma radiation, or even neutron into light. These detectors have two basic areas are the scintillator material, photomultiplier tube, and connector pins which is connected to a counter to recorded a pulses it is in Figure 13.

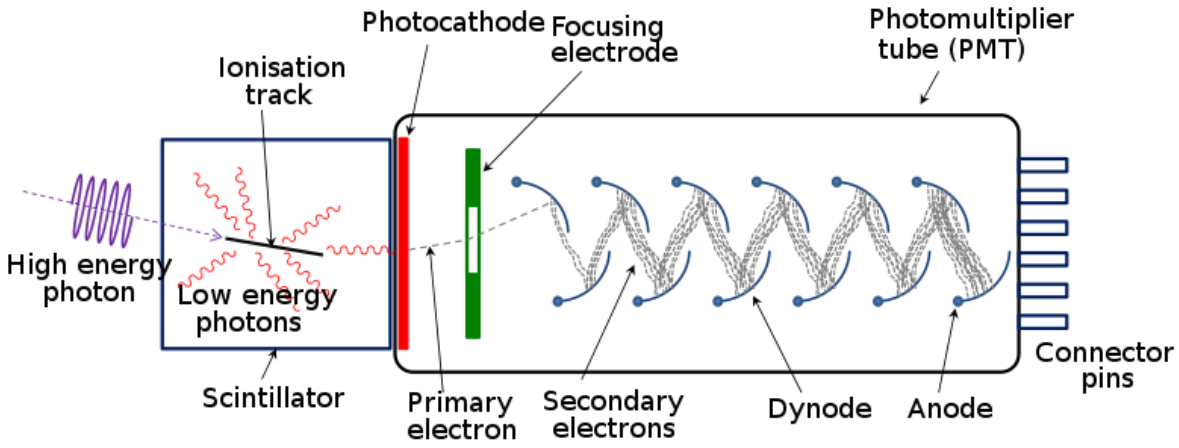


Figure 13: Scintillation detectors [7].

2.3.1.1 *Scintillation detectors mechanism*

When nuclear particle comes to the scintillators usually will excited the electrons from the conduction to a valance band, and when the electron return to its normal state will lead to emission of light which related to the incoming radiation, this light is the key will collide with photocathode and liberated a primary electrons under the photoelectric effect. This primary is directly directed into a photomultiplier tube that is responsible of amplification the primary electrons through the dynodes, which has different voltage, lead to accelerate the electrons and double them until they reach the connectors pins, the number of finale electrons reach probably more the 10^6 electrons.

If the incoming radiation does not has a sufficient energy to excited the electron to the conduction band in special kind of scintillator material, we usually add some impurities in forbidden band which is located between the valance and conduction band, also called activators as it is in Figure 14.

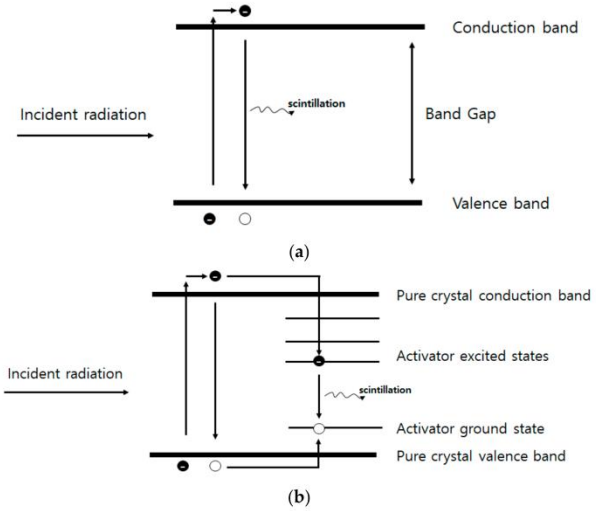


Figure 14: Energy band structure of an inorganic scintillator[9].

2.3.2 Semiconductor detectors

2.3.2.1 *Introduction*

This detectors use a semiconductor material as a material medium that experience the interaction of the incoming radiation. This kind of detectors used widely in spectroscopy and different field of technology. These detectors work with the principle of ionization as ionization chamber, and have a high sensibility of light such as only the incoming radiation need approximately 1eV to jump the electron from the valance to the conduction band or to generate a hole-pair, while gasses detectors need probably 30 eV to ionizing the atoms.

The ionization energy in solids is proportional to the bandgap, so the bandgap sets the minimum detection threshold.

$$E_i = 2.8E_g + 0.6eV, \qquad 2.3$$

Semiconductor materials are distinguished from other materials by their band gap energy, which is roughly equivalent to 1eV, or the energy required to jump an electron from the valance to the conduction band. As demonstrated in Figure 15, the electron becomes free to move about the atoms and conduct electricity. Many key electrical gadgets rely on it as a basic component.

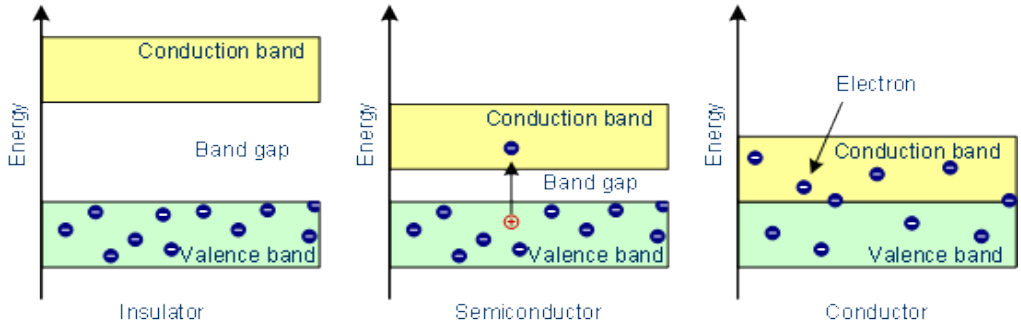


Figure 15: Different between conductors, semiconductors and insulators [9].

[9] https://www.mdpi.com/1996-1073/14/22/7701/htm

2.3.2.2 *Semiconductors types*

To increase the amount of conductivity in a semiconductor material, there are two different ways : by increasing the temperature or adding impurities (doping). These impurities lead to modify the electrical properties and produce other types of semiconductors called P-types or N-types depending on the nature of the valance shells of these impurities.

2.3.2.2.1 Intrinsic semiconductors

Silicon and germanium are the most often used semiconductors, both of which have four electrons in their valance shells, making them pure semiconductors. They differ from one another in a number of ways, as shown in the Table 1. The main reason we pick silicon over germanium is that germanium is so temperature sensitive that we have to build a cooling mechanism to minimize thermal excitation due to its smallest ban gap.

Table 1: Properties of Intrinsic Silicon and Germanium [8].

	Si	Ge
Atomic number	14	32
Atomic weight	28.09	72.60
Stable isotope mass numbers	28-29-30	70-72-73-74-76
Density (300 K); g/cm^3	2.33	5.32
Atoms/cm^3	4.96×10^{22}	4.41×10^{22}
Dielectric constant (relative to vacuum)	12	16
Forbidden energy gap (300 K); eV	1.115	0.665
Forbidden energy gap (0 K); eV	1.165	0.746
Intrinsic carrier density (300 K); cm^{-3}	1.5×10^{10}	2.4×10^{13}
Intrinsic resistivity (300 K); $\Omega \cdot$ cm	2.3×10^5	47
Electron mobility (300 K); cm^2/V $\cdot$ s	1350	3900
Hole mobility (300 K); cm^2/V $\cdot$ s	480	1900
Electron mobility (77 K); cm^2/V $\cdot$ s	2.1×10^4	3.6×10^4
Hole mobility (77 K); cm^2/V $\cdot$ s	1.1×10^4	4.2×10^4
Energy per electron–hole pair (300 K); eV	3.62	
Energy per electron–hole pair (77 K); eV	3.76	2.96
Fano factor (77 K)	0.143 (Ref. 7)	0.129 (Ref. 9)
	0.084 (Ref. 8)	0.08 (Ref. 10)
	0.085 to 0.137 (Ref. 12)	< 0.11 (Ref. 11)
		0.057 to 0.064 (Ref. 12)
	0.16 (Ref. 13)	0.058 (Ref. 14)

Source: G. Bertolini and A. Coche (eds.), *Semiconductor Detectors*, Elsevier-North Holland, Amsterdam, 1968, except where noted.

There is a certain probability of turning the electron into a conduction bond under thermal excitation described mathematically as:

$$p(T) = CT^{\frac{3}{2}} exp\left(-\frac{E_g}{2kT}\right), \quad 2.4$$

where T is the absolute temperature, E_g in the bandgap energy, K is the Boltzmann constant and C is the proportionality constant characteristic of the material.

In addition, in pure semiconductors the number of electrons (n_i) equal the number of holes (p_i) generated either by the ionizing radiation or under thermal excitation:

$$n_i = p_i \quad 2.5$$

2.3.2.2.2 N-Type semiconductors

It is the case when impurities added has extract electron than the need to construct a covalent band with surrounded atoms of pure semiconductor in their valance shells. This extra electron will positioned in forbidden band near the conduction know as a Fermi level. This extra electrons also called donor impurities, as it is shown in Figure 16(b), and may excited into a conduction band just by thermal excitation as it is illustrate in equation (2.3).

For example, a silicon has a four valance electrons (tetravalent impurity), in this case to produce N-type semiconductor, we need to add impurities has a five valance electrons (pentavalent impurity)or element located in Group V of the periodic table as it is shown in Figure 16(a). Notice the charge carriers in N-type semiconductor is electrons

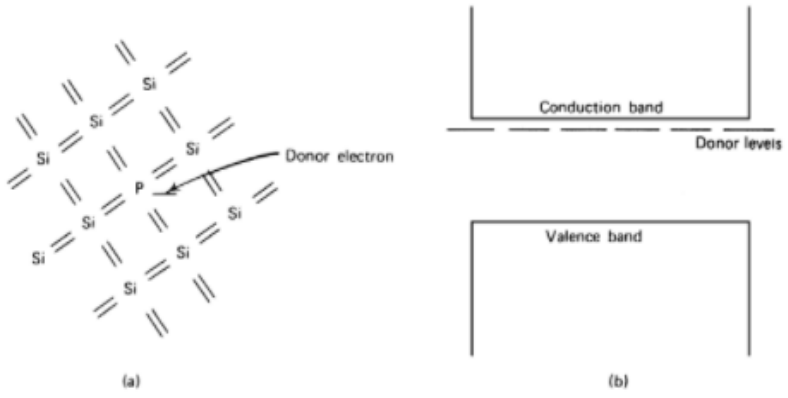


Figure 16: Representation of a donor impurity (phosphorus) occupying a substitutional site in a silicon crystal. (b) Corresponding donor levels created in the silicon band gap [8]

2.3.2.2.3 P-Type semiconductors

It is the case when impurities added do not have a sufficient number of electrons to make a covalent band with surrounded atoms shells of pure semiconductor in their valance shells, this need of electron refers to a hole, this hole is located near the valance band which

create a acceptor level (Fermi level), as is shown in Figure 17(b). Those vacancies (holes) may fill by the thermal excitation of the electron from another covalent band.

For example, a silicon has a four valance electrons (tetravalent impurity), in this case to produce P-type semiconductor, we need to add impurities has a three valance electrons or trivalent impurity or element located in Group III of the periodic table . Notice: the charges carriers in this situation is a holes.

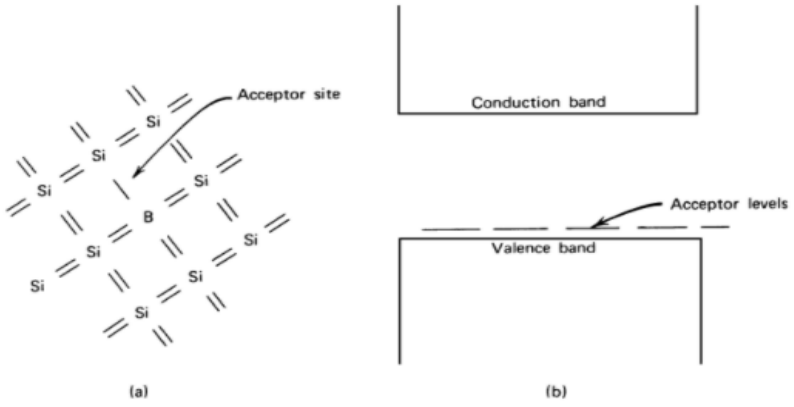


Figure 17: Representation of an acceptor impurity (boron) occupying a substitional site in a silicon crystal .(b) corresponding acceptor levels created in the silicon band gap [8].

2.3.2.2.4 Heavy doped semiconductor

When the pure semiconductor experience a high impurities than the doped semiconductor symbolized as P^+ and N^+ .

2.3.3 Semiconductors as radiation detectors

The combination of different types of semiconductor can make a several devices in different field of technology one of the most important role of those is photodiode works especially when we collect this combination in reverse biased with HV.

2.3.3.1 *PN-Junction*

There is a certain event that can happen when we construct a PN junction. Firstly, there is a certain amount of N-type negative charge moving in the P-type semiconductor, which leads to creating holes in the N-type semiconductor, this process is known as the diffusion (see Figure 18). This new distribution called depletion region also called barrier potential differs from one type of semiconductor to another, for example silicon doped at 0.7 V and germanium doped at 0.3 V.

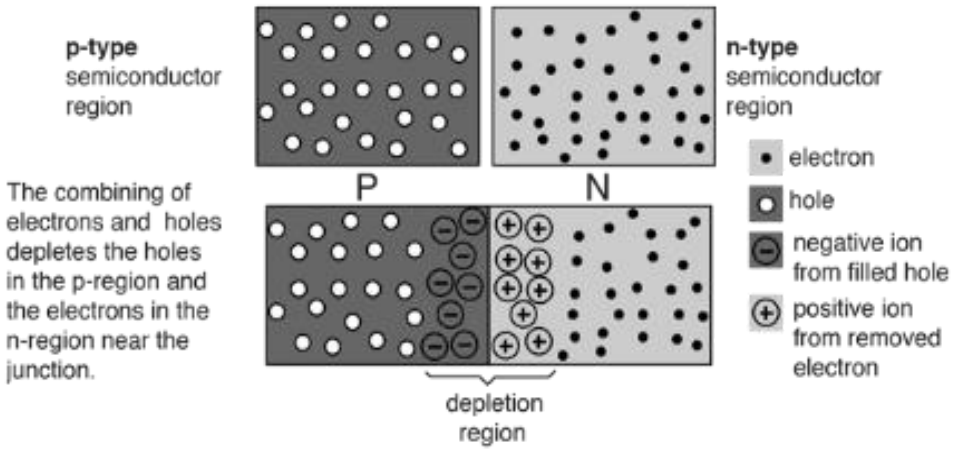


Figure 18: Combination of P and N type semiconductor[10] .

In addition, the energy diagram also experience a change until the PN junction reach the equilibrium or until the formation of the depletion region (see Figure 19).

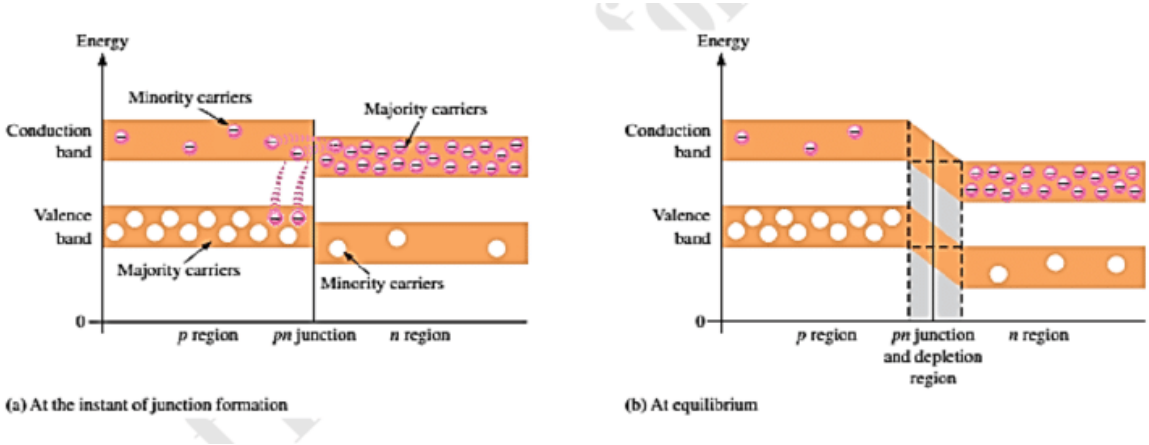


Figure 19: Diagram of energy of PN junction before and after the equilibrium[11].

Notice if the combination between the two layer is similar than the junction called homo-junction, if no it called hetro-junction.

2.3.3.1.1 PN junction + HV

The PN junction sometimes behave as a diode or photodiode depends the nature of collection the junction with the external terminal of the battery.

[10] http://hyperphysics.phy-astr.gsu.edu/hbase/Solids/pnjun.html
[11] https://instrumentationtools.com/energy-diagrams-pn-junction-depletion-region/

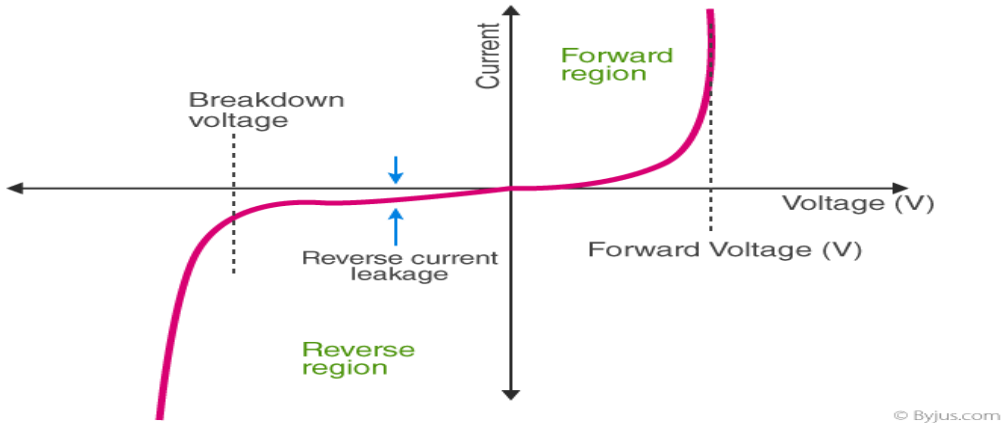


Figure 20: behavior of PN junction +HV[6]

2.3.3.1.1.1 Zero biased (photovoltaic mode)

In this situation the depletion region does not left the current flow through it, the PN junction works as solar cell, which converted the light into an electricity.

2.3.3.1.1.2 Forward biased

Forward biased is the collection of p type semiconductor (also called the anode) with positive terminal of the battery and the collection of N type semiconductor (also called the cathode) with the negative terminal of the battery. In this case, when the predominant role of the PN junction is diode when the applied voltage is high than the barrier potential $V > V_B$ see fig 19 for the reason of decreasing the depletion region, see Figure 21.

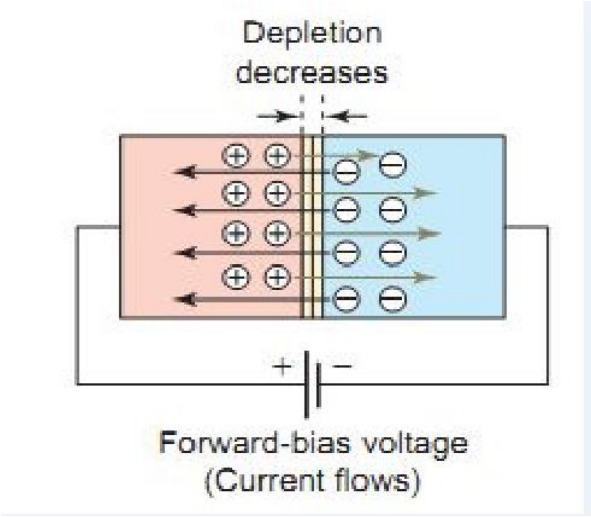


Figure 21: Forward baised mode[12].

2.3.3.1.1.3 Revers biased (photoconductive mode)

Revers biased is the collection of p type semiconductor (anode) with negative terminal of the battery and the collection of N type semiconductor (cathode) with the positive terminal of the

[12] http://www.industrial-electronics.com/electric_mts--cntrl_syst--9.html

battery see fig 20. It is the case when the depletion region increase in its width which lead to stop the current or just few current across the junction due to the influence of opposite charge called revers current leakage (dark current) see Figure 22. The predominant role of PN junction in this situation is photodiode.

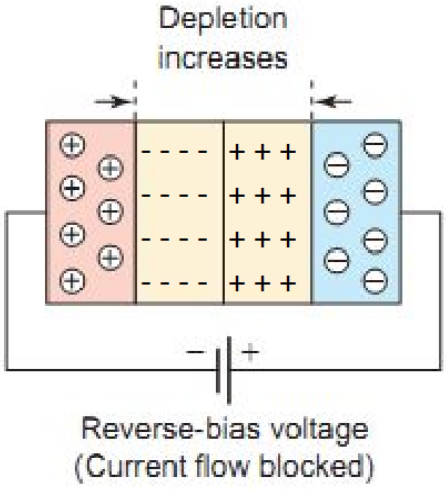


Figure 22: Reverse biased[13].

In addition, from the curve show that the increasing of revers biased lead to break the junction.

When the incoming radiation penetrate within the depletion region will produce a hole pair, and before the electron recombine with a hole, both pair ion accelerated in opposite direction under the electric field force, as the electron drift into N-type and hole drift into P-type due to the influence of opposite charges (see Figure 23).

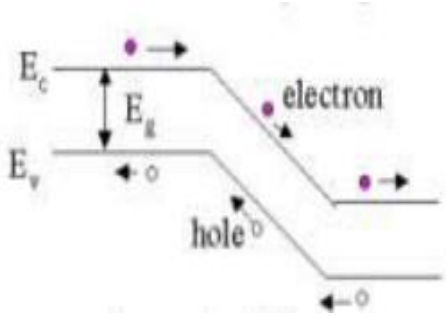


Figure 23: Energy band diagram [10] .

2.3.3.2 *PIN junction*

It is a special kind of PN junction when we add an intrinsic semiconductor between P^+ and N^+ heavy type semiconductor (see Figure 24), in this situation the width of the depletion region becomes equal the width of the intrinsic region.

[13] http://www.industrial-electronics.com/electric_mts--cntrl_syst--9.html

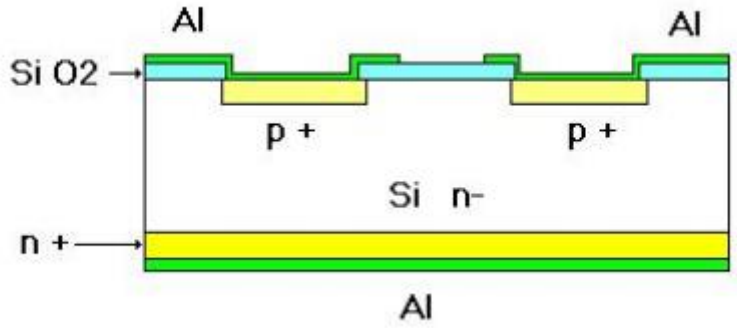


Figure 24: Basic structure of PIN photodiode[11].

In addition, PIN works in both photovoltaic and photoconductive mode (see Figure 25).

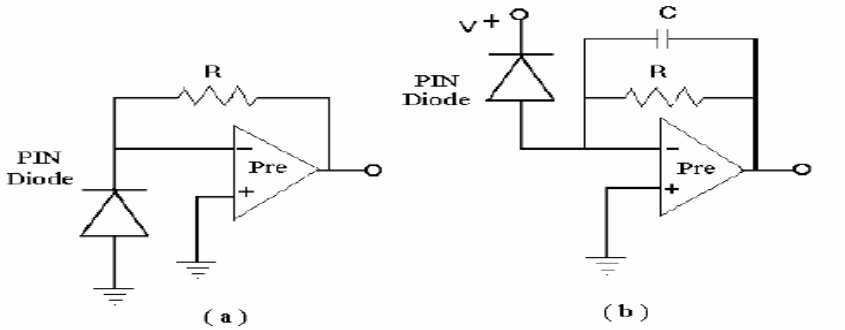


Figure 25: Connections of PIN diode with a preamplifier to operate in: a) photovoltaic mode, b) photoconductive mode.

Pin photodiode work with the same principal of PN junction, the only differences is that the both ions created by the radiation in depletion region would acquire a high energy under the electric field due to the increasing the width of the depletion region lead to maximize the efficiency and minimize the charge collection time.

2.3.3.3 *Surface barrier detector*

SSB made from a thin layer of N-type silicone, which etched by a special kind of acid or alcohol to produce a P-type semiconductor that lead to create an active area, usually we add a peace of gold and aluminum which serve as cathode and anode respectively to decrease the current leakage.

Unlike the PIN diode, surface barrier is characterised by relatively thin dead layers. The sensitivity of surface barriers to light is one of its possible drawbacks. Photons impacting the detector surface can reach the active volume through the thin entrance windows, which are optically transparent. Photon interactions can form electron-hole pairs because the energy of visible light photons is greater than the bandgap energy of most semiconductors (2-4 eV) which influence the detection of interest radiation we usually set up this detector in a darkness place to eliminate this phenomena.



Figure 26 Surface Barrier Detector (photo prise au labo).

2.3.3.4 *Properties of P_N junctions*

2.3.3.4.1 Diffused Junction Detectors

At the point where the n- and p-type impurities reverse their relative positions, a junction(depletion region) is formed some distance from the surface. As a result, a large portion of the surface layer remains outside of the depletion zone, serving as a dead layer or window through which incident radiation must pass before reaching the depletion region. This dead layer can be a serious disadvantage in charged particle spectroscopy because a portion of the particle energy is lost before the active region of the detector is reached. Also The active volume of the detector is represented by the width of the depletion region, which may be modified in partially depleted detectors by changing the reverse bias.

2.3.3.4.2 Leakage current

A minor current on the order of a fraction of a microampere is generally measured when reverse bias is delivered to a junction detector. Internal bulk leakage (leakage current) currents within the detector's volume can be created by one of two mechanisms. The majority carriers could not across the P or N type semiconductor, However, both in cases, the minority carriers are attracted and will be transported across the junction. In most cases, The minority carrier current is low and is rarely a significant source of leakage.

Thermal production of electron-hole pairs within the depletion region is a second source of bulk leakage. This rate will obviously increase as the depletion region grows in size, and it can only be lowered by cooling the material.

2.3.3.4.3 Trapping and Recombination

Charge carriers are lost due to trapping and recombination, which reduces their average lifetime in the crystal.

Once electrons and holes are generated in a semiconductor, they will transit either spontaneously or under the influence of an applied electric field until they are collected at an electrode or recombination occurs. In practice, lifetimes of charge carriers in pure semiconductor before recombination are three or four orders of magnitude smaller than a one second.

For a full detector charge collection, the carriers created by the passage of the incident radiation should be collected before recombination. This condition will hold if the carriers' collection time is short in comparison to their mean lifetime. The collection times is in the order of 10^{-7} to 10^{-8} s and the carrier lifetimes is in the order of 10^{-5} s or more which are usually sufficient.

The trapping is caused by impurities that act as traps for charge carriers in the sense that if a hole or electron is captured, it will be immobilized for a relatively long period of time. Although the trapping center ultimately may release the carrier back to the band from which it came, the time delay is often sufficiently long to prevent that carrier from contributing to the measured pulse which degrade the resolution.

2.3.3.4.4 Rise time

Is the time required to shape the output signal from, usually we prefer to measure it from 10% to 90% see Figure 26 because the time from 0 to 10% is very fast and from 90% to 100% the signal do not experience a significant change. Rise time is very crucial to know if the associated circuit to the detector response to this pulse or not.

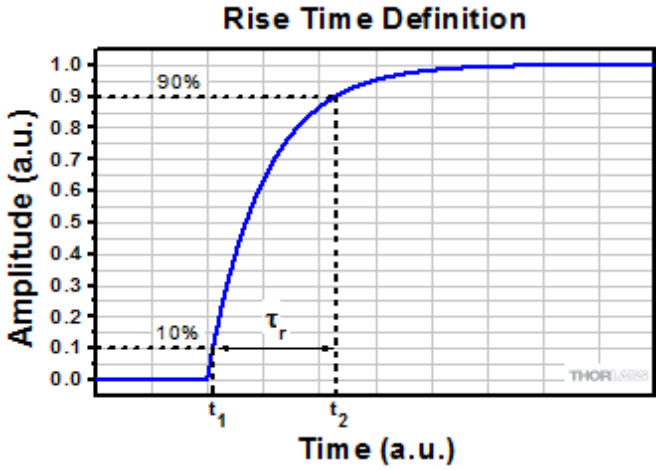


Figure 27 : Rise time[14].

Semiconductor diode detectors are among the fastest of all the conventional radiation detectors. The pulse rise time is on the order of 10 nanoseconds or less. The charge transit time in the depletion region relates to the flow of electrons and holes created by incident radiation across the region of high electric field. The time

[14] https://www.thorlabs.com/newgrouppage9.cfm?objectgroup_id=9817

necessary for complete movement of these charges from their point of production to the opposing extremities of the depletion area limits the rise time of the output pulse. In total, these times are minimized in detectors with high electric fields and small depletion widths, since the depletion width is fixed then the transit time decreases when the bias voltage is increased. However, with partially depleted detectors, the depletion width grows as the bias increases. As a result, a higher bias voltage increases the electric field as well as the distance over which charges must be collected.

2.3.3.4.5 Capacitance

The PN junction act as a capacitance when it collected on revers biased and there is a proportionality between reverse biased and the capacitance is given.

W_d the width of the extend junction is given by:

$$W_d = \sqrt{\frac{2\varepsilon(V_b + V_{bi})}{Ne}} \tag{2.6}$$

where:

N is dopant concentration,

V_{bi} is barrier potential typically 0.5V, ε is the electrical permittivity constant.

Moreover, the values of the capacitance depends on the width of the depletion region:

$$C = \varepsilon \frac{A}{W_d} = A\sqrt{\frac{\varepsilon eN}{2(V_b + V_{bi})}} \tag{2.7}$$

For $V_b \gg V_{bi}$:

$$C \propto \frac{1}{\sqrt{V_b}} \tag{2.8}$$

In the case of PIN junction when we fixed and expend the width of the depletion region (becomes larger), in this case the diode serve as a low capacitance.

Chapter 3

3 Detector Signal Processing

3.1 Electronic associated to detector

Signal processing plays an extremely important role in extracting useful information from detectors current signal. Two important information type are extracted: the amplitude (proportional to the energy) and timing. Typical detector associated chain is sketched in Figure 28. It involve mainly three stages: the preamplifier, the shaping amplifier and the Multi-Channel Analyzer (MCA) which incorporate the analog to digital converter.

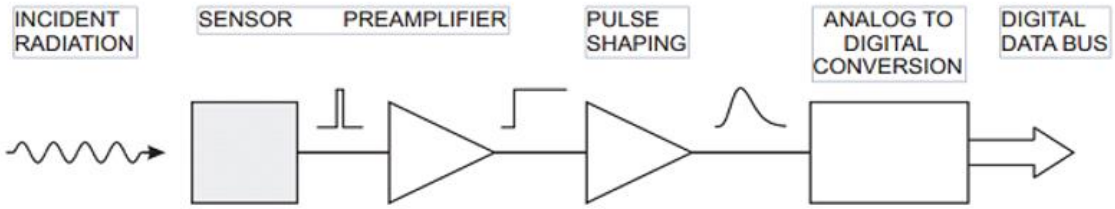


Figure 28 : General Detector chain configuration[12].

3.1.1 Preamplifier.

The Figure 28 show the detector input equivalent circuit, the detector provides a pulse current following the incident radiation interaction. This current is collected at the external circuit and shaped in a form which deliver the type of information needed. We distinguish two mode of operation to represent the signal detector at the output of the preamplifier : the current mode and pulse mode.

3.1.2 Current mode

Generally when the radiation activity is high compared to circuit or detector response, the current mode is used. This method measure the average dc current produced by the interaction between radiation and material medium of detector, as it is show in Figure 29.

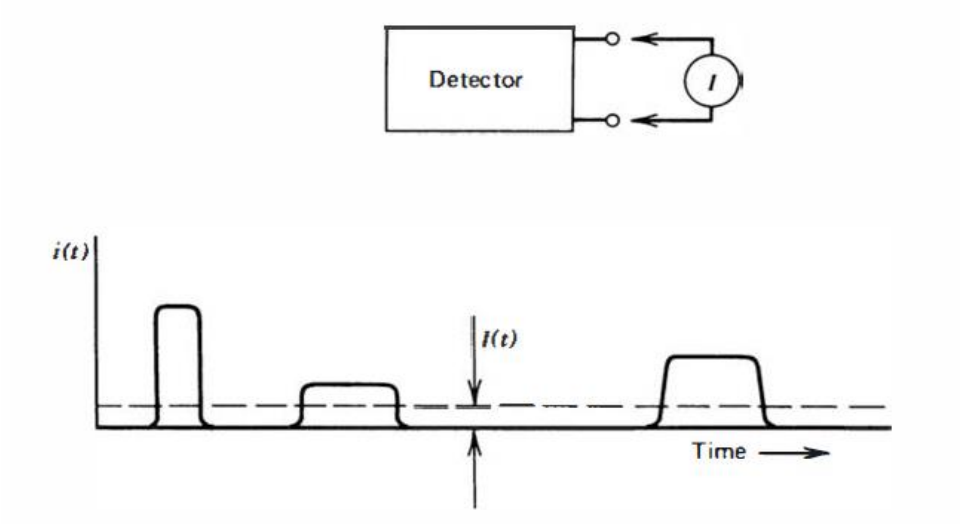


Figure 29 The measure of average current

Mathematically this average current described as:

$$I(t) = \frac{1}{T}\int_{t-T}^{t} i(t)\, dt'. \qquad 3.1$$

T: the average time required to recorded current I .

3.1.3 Pulse mode

This option allows us to study each individual quantum of radiation alone distinguished by its amplitude and shape. This mode is usually affected by the components of the associated circuit (the preamplifier, resistance, and capacitance of the circuit).

The equivalent input detector circuit is shown in Figure 30

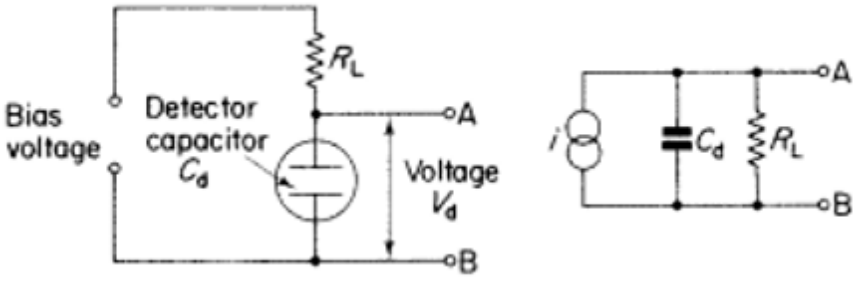
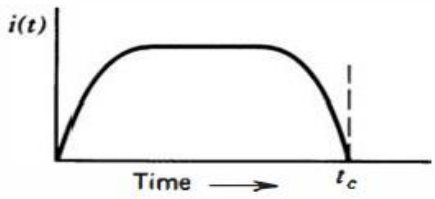


Figure 30 Equivalent Detector Circuit

The current pulse detector has the form sketched in Figure 31



$$\int_0^{t_c} i(t)\,dt = Q$$

Figure 31 : Detector current Pulse.

The shape of the pulse at the output circuit is given by

$$V_C(t) = R_0 I_0 \left(1 - e^{-\frac{t_C}{RC}}\right) \quad for\ t < t_c. \tag{3.2}$$

3.1.3.1 *Case 1* $(\tau = RC) \ll t_c$

In this case we can neglect the exponential term in the equation (3.2) we get therefore:

$$V_C(t) = R_0 I_0 \left(1 - e^{-\frac{t_C}{RC}}\right) \cong R_0 I_0. \tag{3.3}$$

The current flowing through the resistance is equal to the current produced by the interaction within detector. Also the voltage produced in the circuit, appear nearly the same time with the same image of the pulse current detector. Figure 32(b).

3.1.3.2 *Case 2* $(\tau = RC) \gg t_c$

In this case by taking Taylor approximation we get:

$$V_C(t) = R_0 I_0 \left(1 - e^{-\frac{t_C}{R_0 C}}\right) \cong R_0 I_0 \left(1 - \left(1 - \frac{t_C}{R_0 C}\right)\right) = R_0 I_0 \frac{t_C}{R_0 C} = \frac{Q}{C}. \tag{3.4}$$

We deduice:

$$V = \frac{Q}{C} \tag{3.5}$$

.

The signal at the output circuit is proportional to the charge produced within the detector (charge to voltage conversion). The Figure 32 illustrate the two case.

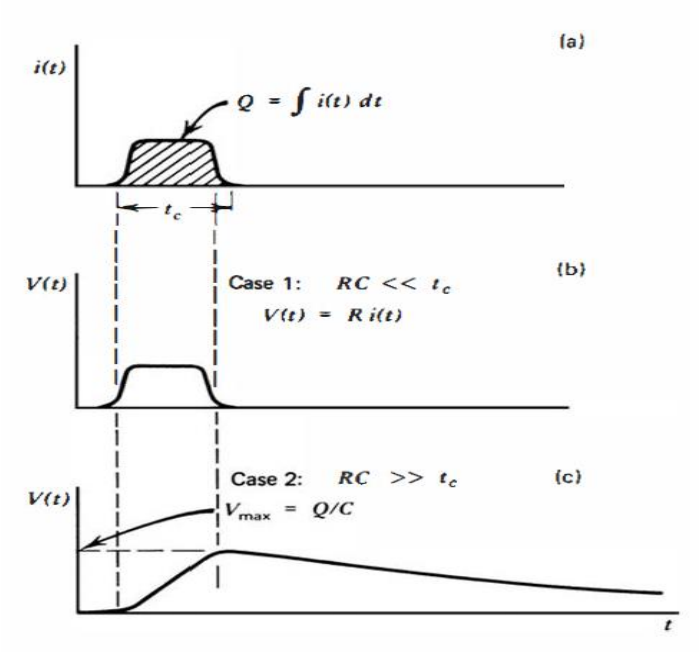


Figure 32: (a) The assumed current output from detector. (b) The signal voltage V(t) for the case of a small time constant load circuit. (c): The signal voltage V(t) for the case of a large time constant load circuit.

We remark in eq.3.4 that the circuit output signal increase with decreasing the capacity that integrate the charge, in other word the sensitivity of the circuit increase by decreasing capacity value. In the simple form of the circuit of Figure 30, the capacitance can vary strongly by any components in the circuit (detector or cable capacitance) which degrade the sensitivity and resolution of the circuit.

The solution to this problem is the use of the circuit sketched in the Figure 33.

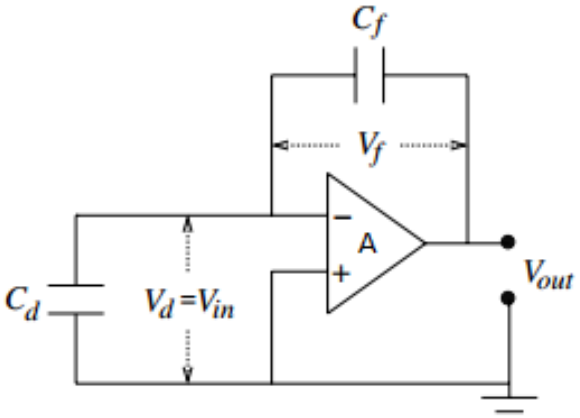


Figure 33 : Typical charge preamplifier configuration

A high open loop gain (A>>) amplifier is used with our capacity of interest used in feedback of the amplifier. In this configuration, the signal at the output keep the value of $\frac{Q}{C_f}$

but here the capacity C_f is virtually insensitive to any input capacitance (detector, stray and parasitic capacitance). This become possible as the feedback capacitance C_f is viewed at the input as C_f times the amplifier open loop gain $C_f(A+1)$. By consequence, all the maximum detector charge is transferred to the feedback capacitance while keeping this capacity as low as possible to increase sensitivity without any effect of other capacitance on the input.

3.1.4 Amplifier:

The signal at the preamplifier output still need other shaping and amplification to extract the energy distribution with a best resolution by increasing signal to noise ratio. The Figure 34 show the general configuration of an amplifier.

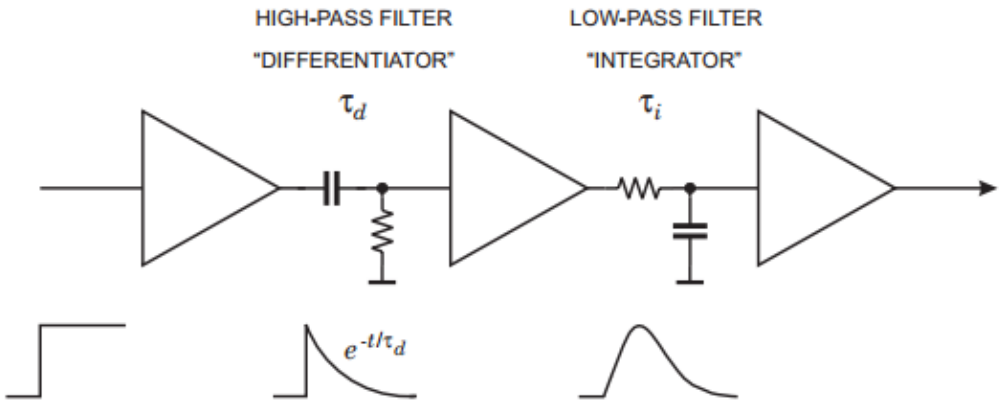


Figure 34 : Configuration of an amplifier

The amplifier involve mainly a low and high pass filter (Figure 34). The high pass filter is referred also as differentiator to reduce the pulse duration and avoiding pile-up in high rate activity. The low pass filter is referred as an integrator that smooth and reduce pulse noise. An extensive study in literature showed that a maximum of signal to noise ratio is achieved when the differentiator and integrator time constant are equal.

3.1.5 ADC Resolution

The ADC device convert the analog value at its input to a binary value at its output. The bit number of the output define the ADC resolution. For example suppose that the input voltage span between 0 and 10 volt and the ADC has a 8 bit binary output, therefore the number of value which the input are divided and converted to numerical value is 28 = 256 value or quantum (10V/256 =39 mV). If we choose 12 bit ADC we obtain 212 = 4096 value or quantum (10V/4096 =2.44mV) and we see that the resolution improve by increasing the ADC bit number.

3.1.6 MCA,

Multichanel canal analyser establish a discretization of the amplitude of the peak shaped pulse at the amplifier output to a successive and cumulative quantum of amplitude proportional to the energie ΔE this discrete amplitude is converted to a numerical value by an

analog to digital converter (ADC). This numerical value for each amplitude become the address of the channel (or the bin) and its content is incremented for each pulse having the same amplitude. This lead to the distribution of incident energy and its rate occurrence which is called spectra.

3.2 Pulse height spectra

It is a way to study a large number of radiations treated by pulse mode, which is special kind of energy distribution shows us the relation between $\frac{dN}{dH}$ and H as it is in Figure 35, where:

dN: Is the differential of pulse number recorded,

dH: Represents the differential amplitude recorded .

From Figure 35, we can deduce several information about the energy of incoming radiation such as the repetition of number of pulse with amplitude between H1 and H2:

$$N = \int_{H_1}^{H_2} \frac{dN}{dH} dH. \qquad 3.6$$

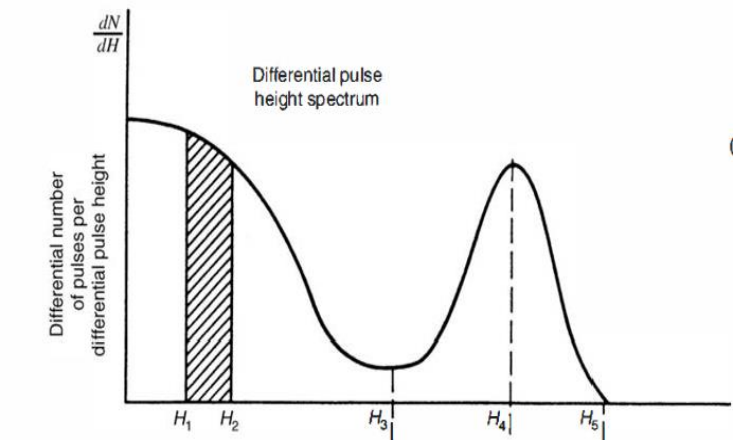


Figure 35: Displaying the differential of height stpectrum[4].

H_3: is the very low amount of pulse have recorded.

H_4: is the very large amount of pulse have recorded.

H_5 is the minimum high pulse without any repetition.

From these we can precise the type and the energy of the incoming radiation

3.3 Energy resolution

One of the most important roles of any detector is to display the energy distribution of incident radiation, which described in term of radiation spectroscopy. This distribution may be accuracy or not depends the quality of the detectors, as it is show in Figure 36.

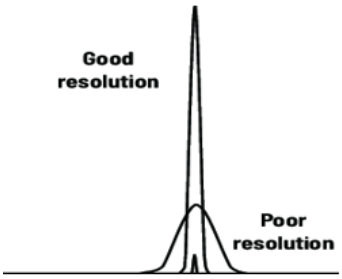


Figure 36: Peak distributions for good and poor energy resolutions [4].

Good resolution (with small width) indicate that the detector is measure the energy radiation with high accuracy, vice versa poor resolution (with large width), the detector measure the energy of incoming radiation with low accuracy or we don't know exactly what the energy of incoming radiation (not distinguish between two radiation).

The energy resolution of any detector described mathematically as:

Resolution $R = \frac{FWHM}{H_0}$ as it is show in Figure 37.

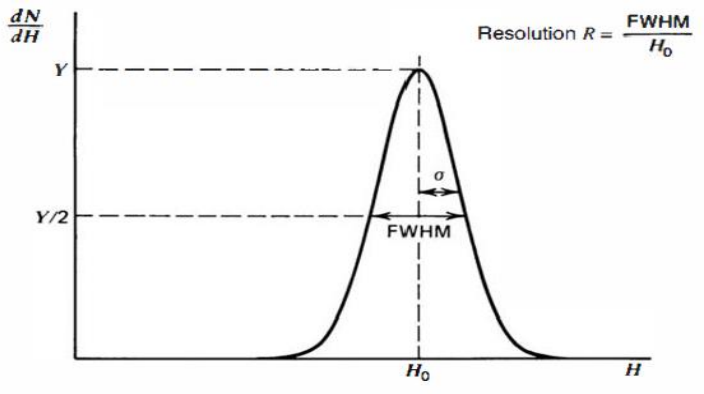


Figure 37: Full Width at Half Maximum (FWHM)[4].

This resolution is ranged from 0 to 100% and varies from detector to detector for example the resolution of gamma ray with semiconductor detectors on generals is 10%.

3.4 Efficiency

The aim of any detector is to record an output pulse when radiation interact within detector, this operation may be affected by several things like the thicknesses of detectors, the level of penetration, or even where the source and detector located. That surly lead us to precise and defined the efficiency of the detectors.
The efficiency conventionally divided into two class absolute and intrinsic efficiency where

$$\varepsilon_{abs} = \frac{number\ of\ pulses\ recorded}{number\ of\ radiation\ quanta\ emitted} \qquad (Absolute)$$

and

$$\varepsilon_{int} = \frac{number\ of\ pulses\ recorded}{number\ of\ quanta\ incident\ in\ detector} \quad (Intrinsic)$$

If the signal coming from the detector controlled by pulse high spectra, then we define the total efficiency (full energy peak efficiency). Which is related of the entire specter recorded (all pulse recorded with different energy), and peak efficiency indicate only the incoming radiation when deposit all its energy, this energy always appear as a peak, as we can see in Figure 38.

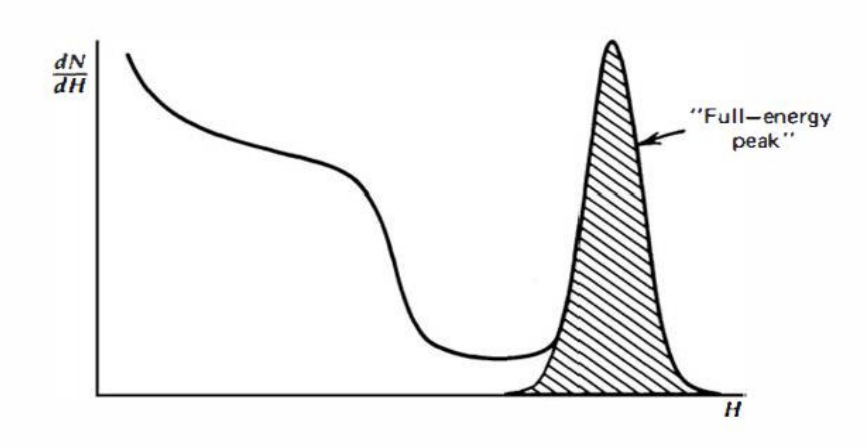


Figure 38: Example of the full-energy peak in a differential pulse height spectrum [4].

The famous relation between these efficiencies is the peak-to-total ratio r:

$$r = \frac{\varepsilon_{peak}}{\varepsilon_{total}} \qquad 3.7$$

Chapter 4

4 OPF430 PIN Photodiode Characterization.

4.1 Introduction

The goal of this part of work is to characterize the PIN photodiode OPF430F in its different aspect. It is encapsulated in a TO-18 package Figure 39. Its features is given in the Table 2.



Figure 39: OPF430F photodiode ; (a) with package (b) electrical symbol

Table 2 : Electrical charactiristic

Maximum Reverse Voltage						100 VDC
Electrical Characteristics (T_A = 25° C unless otherwise noted)						
SYMBOL	**PARAMETER**	**MIN**	**TYP**	**MAX**	**UNITS**	**TEST CONDITIONS**
R	Responsivity	0.45	0.55		A/W	V_R = 5.0V; 50/125µm fiber; λ = 850nm
I_D	Dark Current		0.1	5.0	nA	V_R = 5.0V
λ_p	Peak Response Wavelength		905		nm	
t_r	Output Rise Time		2.0		ns	V_R = 5V; R_L = 50W, 10%-90%
C_T	Total Capacitance		1.5	2.0	pF	V_R = 5V
FoV	Field of View		80		deg	

4.2 Experimental banc

Two experimental banc was set up. The first is intended to collect the dark current, the second is intended to get the energy distribution (spectra) of the radiation particle and timing property (signal shape and speed) of the signal detector.

A support for PIN photodiode and the radiation source was designed and manufactured in the mechanical workshop although, this support was not convenient for alpha particle test because this charged particle need a vacuum medium, therefore this support was replaced by an adapted one used with the barrier surface detector showed in Figure 41.



Figure 40 : Support of radiation source.

Conceived support with polyethylene materiel. The duplicated discs showed in (a) are used to vary the distance of the source from the PIN photodiode detector.

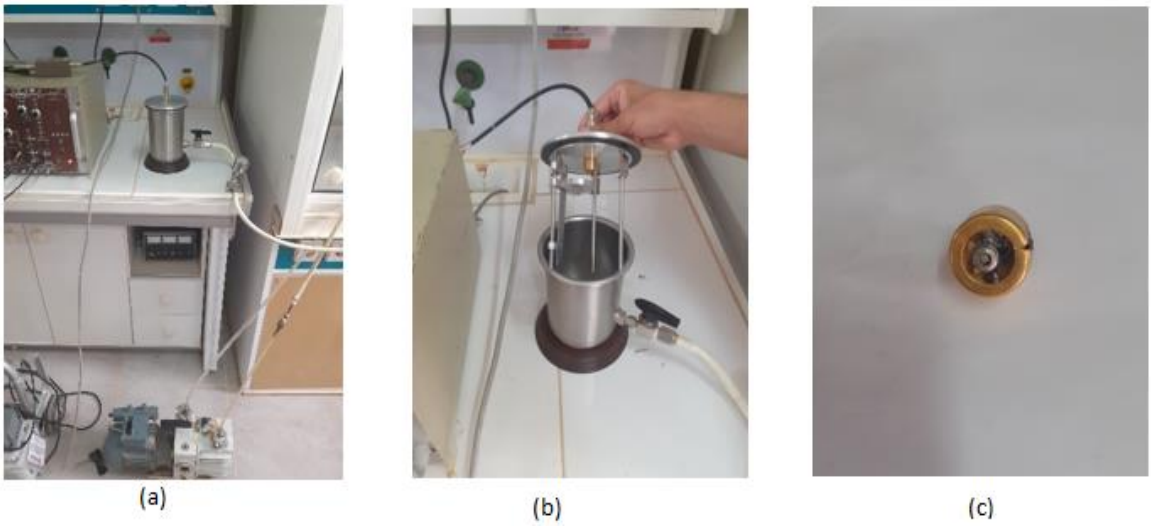


Figure 41: Alpha particle support and vacuum : (a) A general view with the pump vacuum, (b) an inside view of the enclosure with barrier surface detector attached at the center of the cover of the enclosure, (c) PIN photodiode adapted to the barrier surface detector support.

4.3 Leakage (or Dark) current

We use a low current measurement apparatus, the keithly 617 electrometer capable of measuring a very low current (below than Pico-ampere). The measuring circuit is sketched in Figure 42 : Leakage current measurment circuit. At the right the keitly 617 electrometer.

The photodiode window was covered by a dark stripe to avoid visible light induced current. We increase the voltage by a step of 10 volt and we record the different current value displayed in Table 3 .

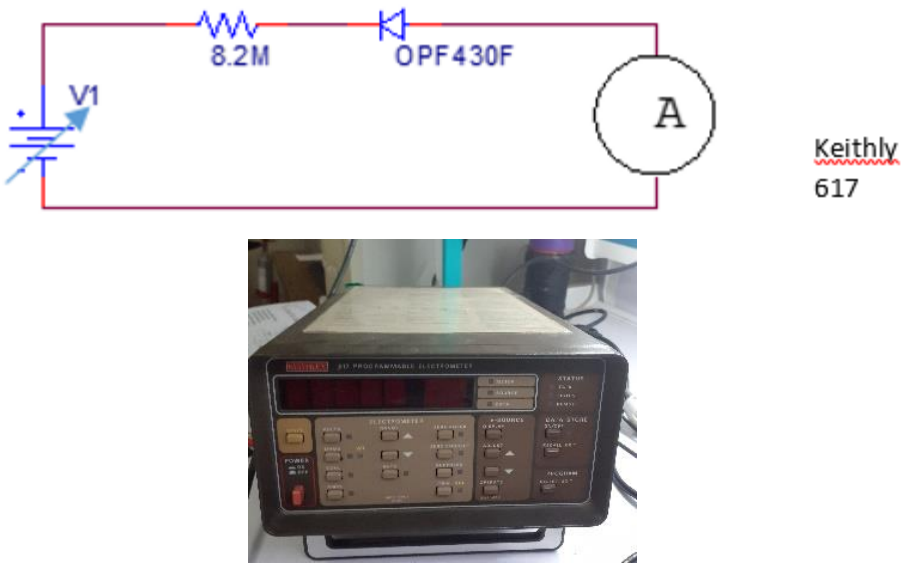


Figure 42 : Leakage current measurment circuit. At the right the keitly 617 electrometer.

Table 3 : Revers biased VS leakage current

V(volt)	I(pA)
18,44	25
30	28
40	30,3
50	33
60	36
70	40,2
80	46,5
90	59,23
100	93,5

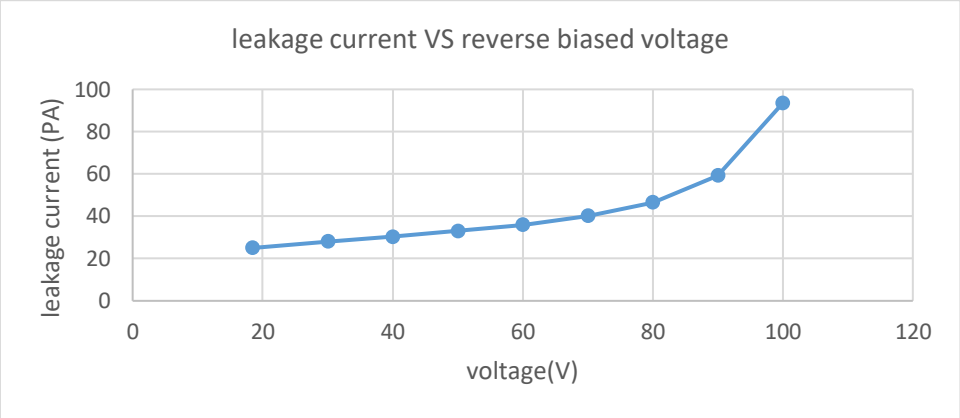


Figure 43 : Leakage current

We can notice the very low dark current value (36 pA at 60 volt). The current grow quickly from 85 volt. At 100 volt we can confirm the maximum reverse voltage limit given in the photodiode datasheet (Table 2).

4.4 Photodiode Capacity.

The OPF430F photodiode has a very low junction capacitance (see datasheet in Table 2). This made its experimental measure somewhat difficult (with respect to time constraint dedicated to this project)

4.5 Alpha radiation measurement

4.5.1 Experimental Banc

The OPF430F pin photodiode will be tested in its spectral and timing aspect. The **Figure 44** show the instrumentation chain used for this purposes. The various modules in this chain are the detector high voltage bias, the preamplifier, the amplifier and the MCA. The oscilloscope is used for observing the signal shape and timing.

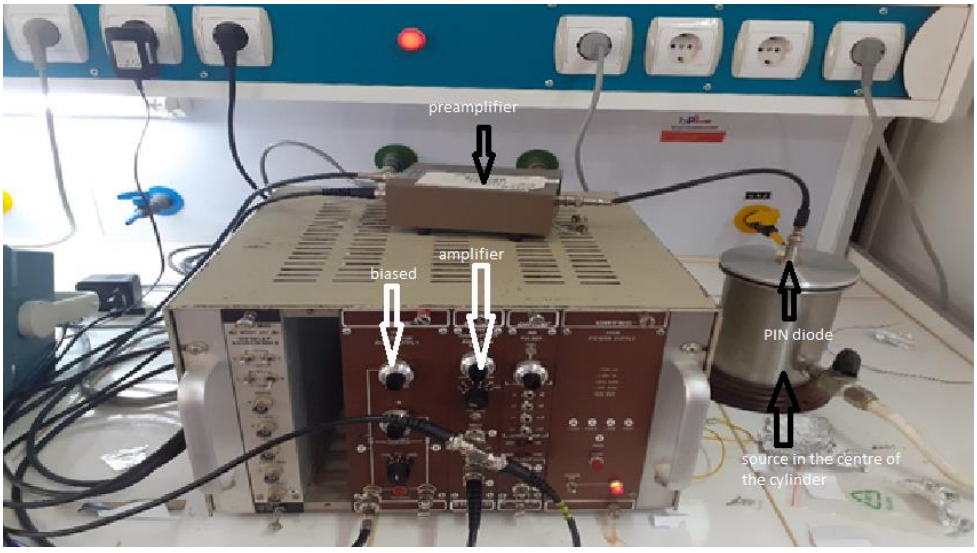


Figure 44: The used detection chain. The MCA and the oscilloscope are not visualized**.**

4.5.2 Radiation Source.

We used the Am241 and PU239 source Figure 45 The primary peak energy of alpha particles and low gamma energy of the source are included in the Table 4.



Figure 45: Am-241-Pu-239 Radiation source

Table 4: Energy liberated by AM-241 and Pu-239

Source	Date of fabrication	Activity (KBq)	Most probable Peak energy (MeV)	Probability
Am-241 with Half-life: $432Y_r$	30-10-2015	1.446	5.48 MeV- alpha 13.6 keV- gamma rays	0.85 0.44
Pu-239 with Half-life: $24.111Y_r$	30-10-2015		5.15 Mev- alpha	0.733

4.5.3 Experimental Protocol

For an adequate characterization of the OPF430 photodiode and to highlight the influence of some semiconductor parameters on its features (resolution, efficiency, speed), we have adopted an experimental protocol, which consist of:

- The use of the barrier surface detector for comparison purposes.

- Measurements will be taken with and without bias voltage.

- Spectral energy distribution acquisition.

- Preamplifier output signal acquisition.

4.5.4 Signal Acquisition.

4.5.4.1 *OPF430 PIN Photodiode Signal Acquisition.*

The Figure 46 shows the signal rise time at the output of the preamplifier which correspond to the detector charge collection time with and without polarization.

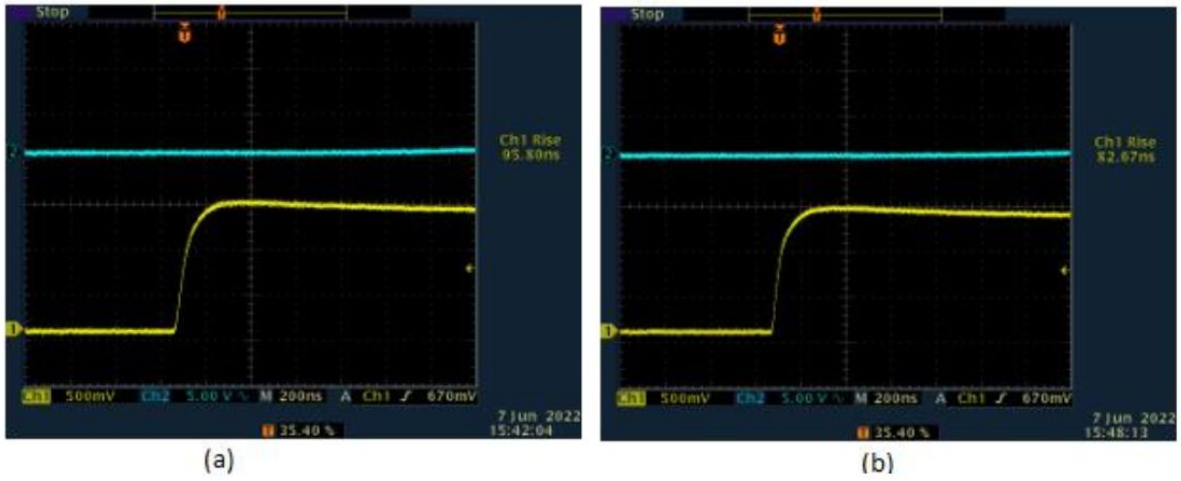


Figure 46 : Rise time at the preamplifier output : (a) without voltage biasing; (b) with voltage biasing.

4.5.4.2 *Barrier surface Signal Acquisition.*

The Figure 47 show the signal rise time at the output of the preamplifier which correspond to the detector charge collection time with and without polarization.

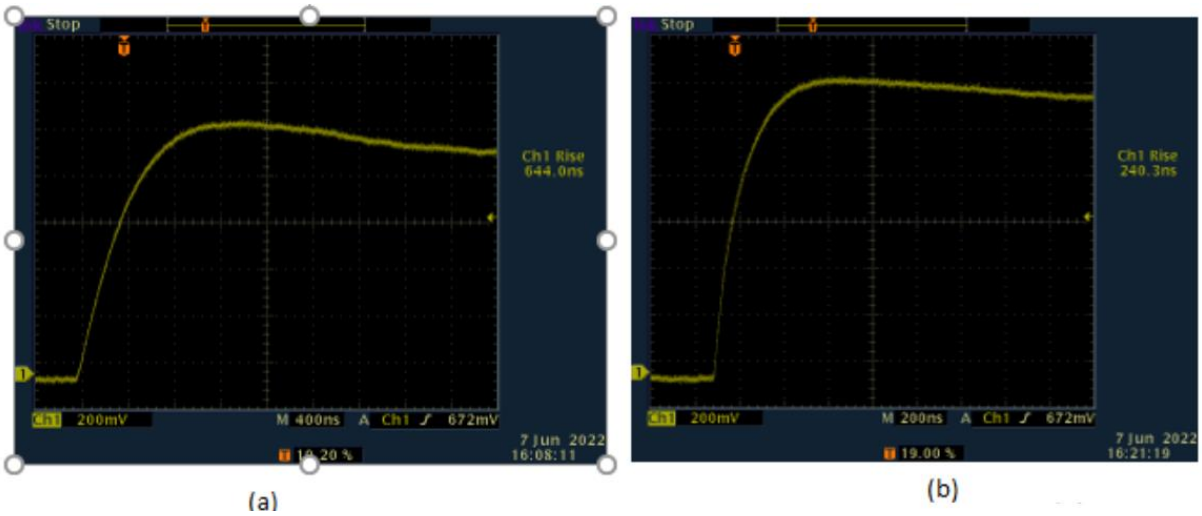


Figure 47 : Rise time at the preamplifier output : (a) Without voltage biasing (b) With voltage biasing,.

4.5.4.3 *Results discussion*

As we can see, in both detectors the voltage biasing reduces the rise time that reflect the charge collection time. The bias voltage speed up the hole-electron pair collection. We remark a slight rise time reduction in PIN photodiode (14%) detector compared to the barrier surface detector (62%). This is due to thickness of the semiconductor wafer and therefore the

depletion layer. This difference in thickness (depletion layer length) make a difference in time collection favorited by bias voltage.

4.6 Spectra Acquisition

4.6.1 OPF430 PIN Photodiode Spectre Acquisition.

The OPF430 photodiode's glass windows were removed to prevent alpha charged particle stopping. The acquired spectre is displayed in Figure 48 and smoothed and zoomed in Figure 49.

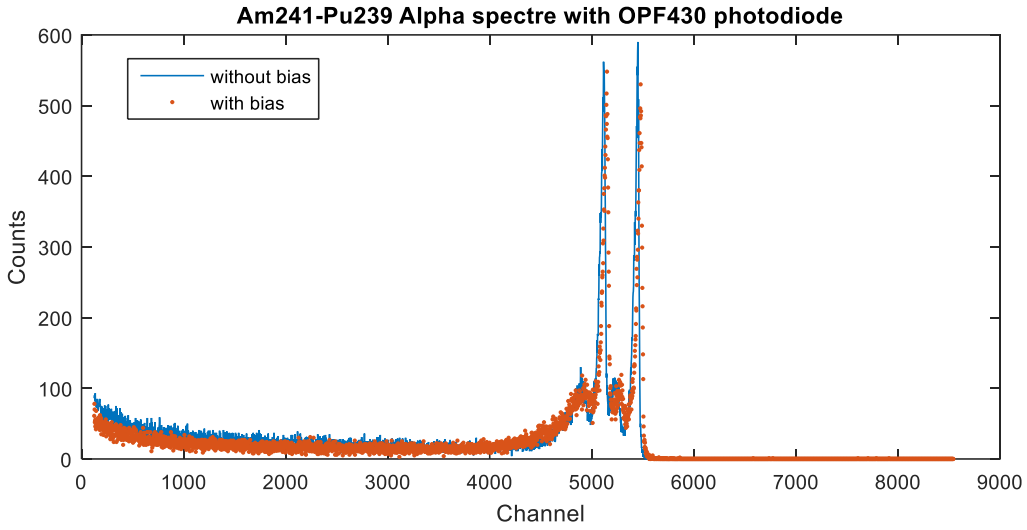


Figure 48 Am241- Pu239 Alpha spectra with OPF 430 photodiode

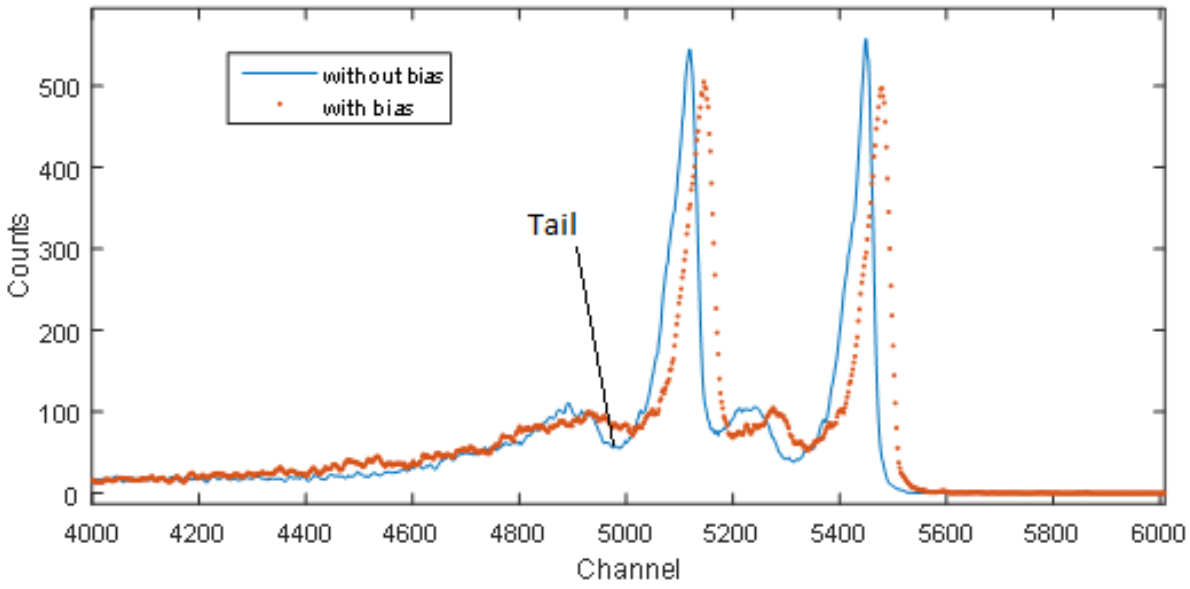


Figure 49 : OPF430 PIN Photodiode (zoomed) spectre with and without biased voltage. The tail in the non polarized spectre is due to the trap effect [6].

4.6.2 Barrier Surface Spectre Acquisition.

The spectrum is displayed in Figure 50 below:

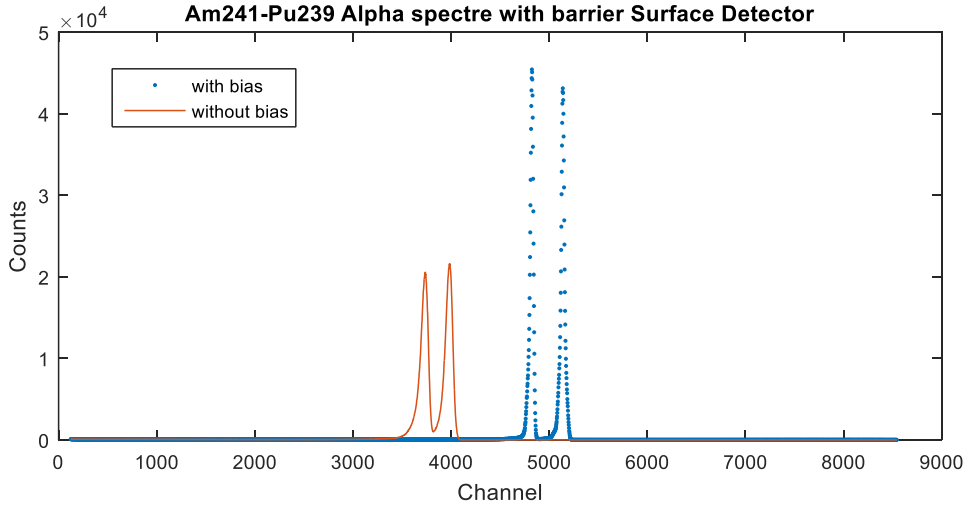


Figure 50 : Am241-PU239 alpha spectra with SSB

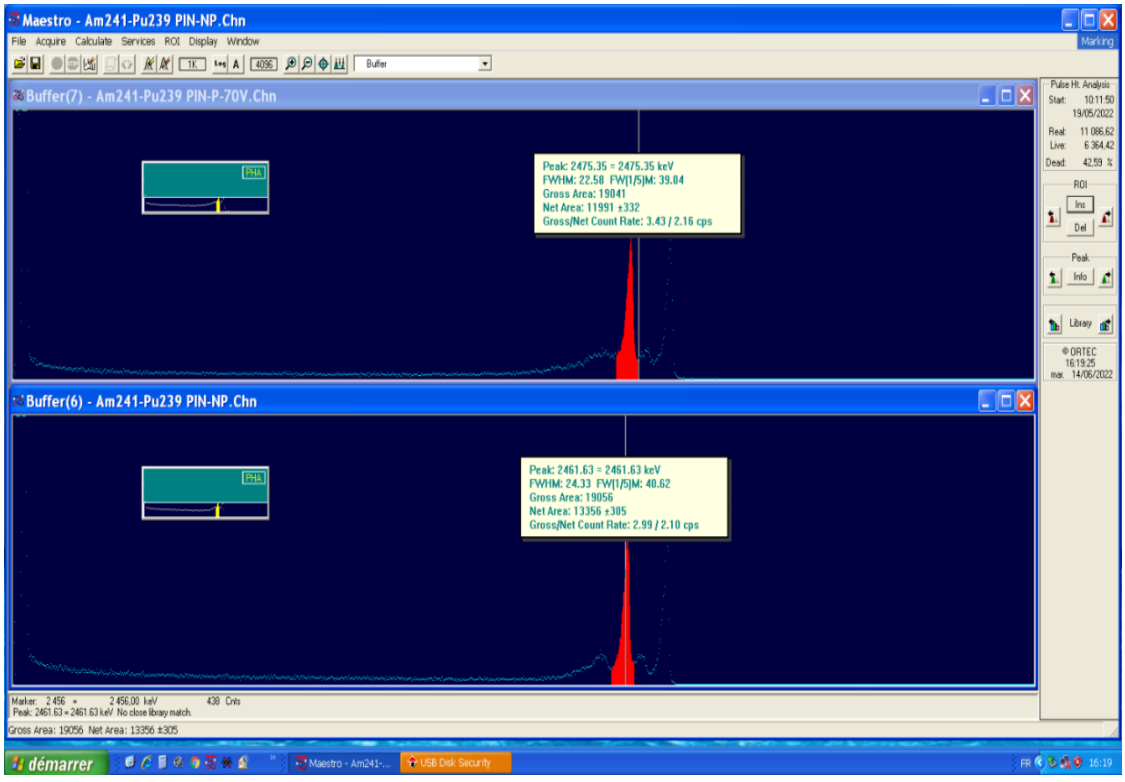


Figure 51 : PIN photodiode spectrum displayed by MCA firmeware with spectrum features.

The MCA energy calibration give (by using the two peak energy in Table 5)

Table 5 : Relation between channel and energy

channel	energy(keV)
2392	5150
2551	5480

$$\mathrm{E(keV)} = 2.07 * x + 185 \; where \; x(in \; channel \; number)$$

We get the respective resolution for 5.48 MeV peak (FWHM) in Table 6.

Table 6 resolution for both spectrum(with and without HV)

	Non Polarized (keV)	Polarized (keV)
PIN photodiode	38.43	45
Surface Barrier	83	36

4.6.3 Result discussion

First we can notice the relative good resolution of the pin photodiode (45 keV) compared to the surface barrier detector (36keV). For alpha particle of 5.48MeV energy, the theoretical resolution is 3.47 keV and in practice tends to be no better than 10 keV [6].

We can notice also the net difference between PIN photodiode and surface barrier detector due to their inner structure (thickness and the presence of dead layer). There is a slight shift in PIN OPF430 spectrum after polarization due to the reduction of recombination pair compared to surface barrier.

4.7 Spectroscopy of gamma ray at low energy

For the reason of the capacitance limit used in preamplifier (0.1pF), the signal produce with gamma rays has energy 13.6 keV is very weak and theoretically describe as:

The number of holes pairs produce by ionizing radiation in silicone is:

$$N = \frac{E}{3.6} \qquad 4.1$$

The charge Q produced by ionizing radiation is proportional to the incoming radiation such as:

$$Q = N.e \qquad 4.2$$

The signal creates due to the incoming radiation is:

$$V = \frac{Q}{C} \qquad 4.3$$

For gamma rays has energy 13.6 keV:

$$V = \frac{13.6 * 10^3 * 1.6 * 10^{-19}}{3.6 * 0.1 * 10^{-12}} = 6.04\ mV \qquad 4.4$$

The value of 6.04 mV is the signal produced by the incident gamma rays. We know theoretically for this kind of radiation that in the experiment only a fraction of this charge is available, half in the optimal case"[13]. It becomes 3.02 mV in our case. So, it is very low and for this reason we cannot have a satisfactory signal displayable on the MCA.

The Figure 52 show the gamma signal acquired by the OPF430 photodiode and we remark that is partially burried in noise.

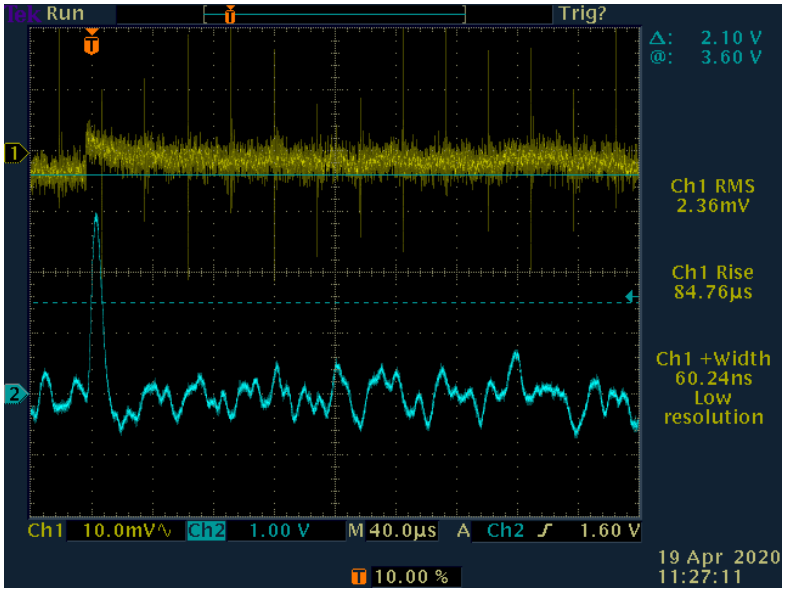


Figure 52 : Gamma signal at the preamplifier output (upper) and the corresponding amplifier output (down). The signal need more preamplification to be useful.

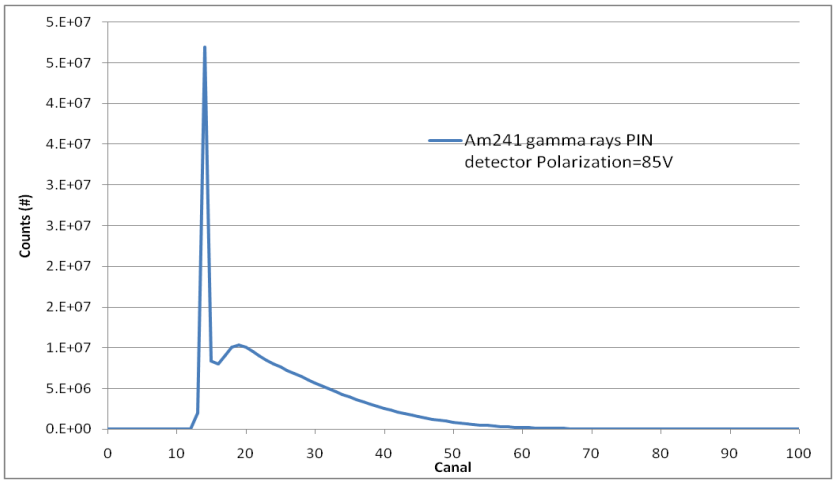


Figure 53 : Low energy gamma rays spectra acquired by OPF430 PIN photodiode : the noise is dominant.

To rise the amount of signal we have to build a high sensitivity preamplifier with special topology [14].

Chapter 5

5 Monte Carlo Simulation study

5.1 Introduction

In a term of interaction between radiation and matter the incoming radiation may experience a several phenomenon during its transportation like absorption, dispersion, losing of energy, or even create secondary particles depends the nature of particle, the energy of particle, nature of interaction, and even the surrounding environment. The best way to simulate the behavior of particles during its movements is Monte Carlo programs by its various codes like EGS, ITQ, MORSE, MCNP, SRIM, TRIPOLI, GEANT etc.

In our study, we will focus on the study of MCNP version 5, and SRIM codes. First MCNP5 on general used to study the interaction of electrons, thermal-fast neutrons, and photons with matter. It developed by Los Alamos laboratory in USA, as it becomes able to study the photon has energy ranged from 1keV to 1GeV, this development continued until the MCNP5 become an important part of different field of technologies like medical, military, dosimeter, and without forgetting transportation of particles. Secondly, SRIM Monte Carlo used mainly for studying the target of charged particle that mainly used as a tool of calculation, this code has written and developed by a Canadian group in Quebec.

In a term of history, Monte Carlo is name of huge place of gambling, scientist at that time inspired this name when they tried to solve the problem of neutron's transportation, they create a method based on the statics and probability.

5.1 MCNP structure and mechanism of working

MCNP as any program has input file to define the problem and the output file to get the result of the study. The input file constructed from three main areas is cells card, surface card, and data card respectively see Figure 54. Each card has a significant role to define the problem.

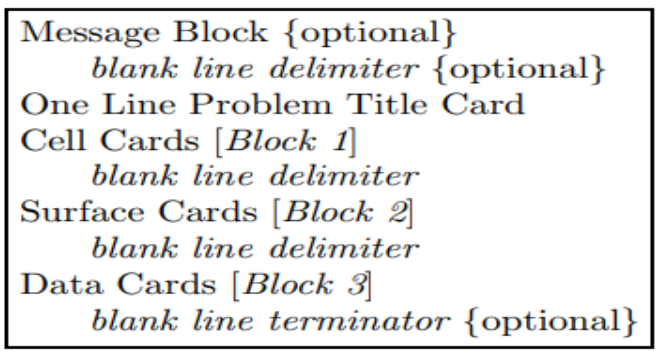


Figure 54: Structure of input file of MCNP [15].

5.1.1 Surfaces

It is very important to discuss first about the surfaces despite it's located after the cells card in the structure of MCNP program. Because the cells are made by the thanks of surfaces, it's the main part of constructing the shape of our study like detector, or reactor. The most common surfaces are gathered in Table 7:

Table 7: MCNP Surface Cards[13]

Mnemonic	Type	Description	Equation	Card Entries
P	plane	general	$Ax + By + Cz - D = 0$	$A\ B\ C\ D$
PX		normal to x-axis	$x - D = 0$	D
PY		normal to y-axis	$y - D = 0$	D
PZ		normal to z-axis	$z - D = 0$	D
SO	sphere	centered at origin	$x^2 + y^2 + z^2 - R^2 = 0$	R
S		general	$(x-\bar{x})^2+(y-\bar{y})^2+(z-\bar{z})^2-R^2=0$	$\bar{x}\ \bar{y}\ \bar{z}\ R$
SX		centered on x-axis	$(x - \bar{x})^2 + y^2 + z^2 - R^2 = 0$	$\bar{x}\ R$
SY		centered on y-axis	$x^2 + (y - \bar{y})^2 + z^2 - R^2 = 0$	$\bar{y}\ R$
SZ		centered on z-axis	$x^2 + y^2 + (z - \bar{z})^2 - R^2 = 0$	$\bar{z}\ R$
C/X	cylinder	parallel to x-axis	$(y - \bar{y})^2 + (z - \bar{z})^2 - R^2 = 0$	$\bar{y}\ \bar{z}\ R$
C/Y		parallel to y-axis	$(x - \bar{x})^2 + (z - \bar{z})^2 - R^2 = 0$	$\bar{x}\ \bar{z}\ R$
C/Z		parallel to z-axis	$(x - \bar{x})^2 + (y - \bar{y})^2 - R^2 = 0$	$\bar{x}\ \bar{y}\ R$
CX		on x-axis	$y^2 + z^2 - R^2 = 0$	R
CY		on y-axis	$x^2 + z^2 - R^2 = 0$	R
CZ		on z-axis	$x^2 + y^2 - R^2 = 0$	R
K/X	cone	parallel to x-axis	$\sqrt{(y-\bar{y})^2 + (z-\bar{z})^2} - t(x-\bar{x}) = 0$	$\bar{x}\ \bar{y}\ \bar{z}\ t^2\ \pm 1$
K/Y		parallel to y-axis	$\sqrt{(x-\bar{x})^2 + (z-\bar{z})^2} - t(y-\bar{y}) = 0$	$\bar{x}\bar{y}\ \bar{z}\ t^2\ \pm 1$
K/Z		parallel to z-axis	$\sqrt{(x-\bar{x})^2 + (y-\bar{y})^2} - t(z-\bar{z}) = 0$	$\bar{x}\bar{y}\ \bar{z}\ t^2\ \pm 1$
KX		on x-axis	$\sqrt{y^2 + z^2} - t(x - \bar{x}) = 0$	$\bar{x}\ t^2\ \pm 1$
KY		on y-axis	$\sqrt{x^2 + z^2} - t(y - \bar{y}) = 0$	$\bar{y}\ t^2\ \pm 1$
KZ		on z-axis	$\sqrt{x^2 + y^2} - t(z - \bar{z}) = 0$	$\bar{z}\ t^2\ \pm 1$
			± 1 used only for 1-sheet cone	
SQ	ellipsoid hyperboloid paraboloid	axis parallel to x-, y-, or z-axis	$A(x - \bar{x})^2 + B(y - \bar{y})^2 + C(z - \bar{z})^2 + 2D(x - \bar{x}) + 2E(y - \bar{y}) + 2F(z - \bar{z}) + G = 0$	$A\ B\ C\ D\ E\ F\ G\ \bar{x}\ \bar{y}\ \bar{z}$
GQ	cylinder, cone ellipsoid paraboloid hyperboloid	axis not parallel to x-, y-, or z-axis	$Ax^2 + By^2 + Cz^2 + Dxy + Eyz + Fzx + Gz + Hy + Jz + K = 0$	$A\ B\ C\ D\ E\ F\ G\ H\ J\ K$
TX	elliptical or circular torus. Axis is parallel to x-, y-, or z-axis	$(x-\bar{x})^2/B^2 + (\sqrt{(y-\bar{y})^2 + (z-\bar{z})^2} - A)^2/C^2 - 1 = 0$		$\bar{x}\ \bar{y}\ \bar{z} A\ B\ C$
TY		$(y-\bar{y})^2/B^2 + (\sqrt{(x-\bar{x})^2 + (z-\bar{z})^2} - A)^2/C^2 - 1 = 0$		$\bar{x}\ \bar{y}\ \bar{z} A\ B\ C$
TZ		$(z-\bar{z})^2/B^2 + (\sqrt{(x-\bar{x})^2 + (y-\bar{y})^2} - A)^2/C^2 - 1 = 0$		$\bar{x}\ \bar{y}\ \bar{z} A\ B\ C$

5.1.1 Cells card

Cell is the union, intersection or components of many regions (surfaces) to get a special volume or a part of the shape of the interest devices or where the problem is. This section in

MCNP used to define the cells by a special form such as their number, density, geometry, and their importance respectively, positioned in the first card in the structure of MCNP as:

A m d geom. Imp:x=1

Where

A: cell number

m: material number

d: density of the material

geom.: specified the location of cell between its surrounding surfaces

imp:x the importance of the of the cellule usually either equal 1 or 0, 0 refers to the vacuum

Notice there is an alternative way to define the surfaces and cells, known as macrobadies see manually guide MCNP it's very easy.

5.1.2 Data specification

This block will persist the problem and control the result by specify the type of material, radiation source with its energy and the type of result know as tally.

5.1.2.1 *Material specification*

This card will define the type of material that we have discuss in block 1, but not include the density of this material. Usually used the notation ZZZ.AAA.nnx called ZAID, where z is the atomic number and A is atomic mass number, while nn is the cross section of interaction, and x refers to the class of data it may be: C, D, T, Y, and P.

Where

C: continuous energy

D: is discrete reaction

T: is thermal

Y: dosimetry

P: is photon

5.1.2.2 *Source of radiation*

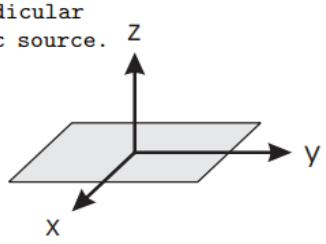
The command SDEF is the key to persist the type of radiation that you want to define, this command always has followed by several variable to more persist the radiation like energy, location of the source, weight of particle, ext. All of this related variable is gathered in the Table 8.

Table 8: Source variables for the SDEF command.

Variable	Meaning	Default
CEL	cell	determined from XXX, YYY, ZZZ and possibly UUU, VVV, WWW
SUR	surface	0 (means cell source)
ERG	energy (MeV)	14 MeV
DIR	μ, the cosine of the angle between VEC and UUU, VVV, WWW. The azimuthal angle is always sampled uniformly in $[0, 2\pi]$	Volume case: μ is sampled uniformly in $[-1.1]$ (isotropic). Surface case: $p(\mu) = 2\mu$ for $\mu\epsilon[0, 1]$ (cosine distribution).
VEC	reference vector for VEC	Volume case: required unless isotropic. Surface case: vector normal to the surface with sign determoined by NRM.
NRM	sign of the surface normal	+1
POS	reference point for positioning sampling	0, 0, 0
RAD	radial distance of the position from POS or AXS	0
EXT	Cell case: distance from POS along AXS. Surface case: cosine of angle from AXS	0
AXS	reference vector for EXT and RAD	no direction
X	x-coordinate of position	no X
Y	y-coordinate of position	no Y
Z	z-coordinate of position	no Z
CCC	cookie-cutter cell	no cookie-cutter cell
ARA	area of surface (required only for direct contributions to point detectors from a plane surface source	none
WGT	particle weight	1
EFF	reference efficiency criterion for position sampling	0.01
PAR	type of particle source emits	= 1 (neutron) if MODE N or P or N P E; = 2 (photon) if MODE P; = 3 (electron) if MODE E

For example if we want to define a plane source, perpendicular to z axis with x=10cm and y=15cm

```
c --- rectangular plane source centered on the origin and perpendicular
c     to the y-axis.  This uses a degenerate Cartesian volumetric source.
c
SDEF  POS=0 0 0   X=d1 Y=d2 Z=0   PAR=2   ERG=1.25
SI1   -10 10      $ sampling range Xmin to Xmax
SP1    0  1       $ weighting for x sampling: here constant
SI2   -15 15      $ sampling range Ymin to Ymax
SP2    0  1       $ weighting for y sampling: here constant
```



5.1.2.3 *Tallies*

This command symbolize in MCNP by F_n to persist the type of result such as efficiency, energy deposit, surface current, ext. depends the need of our study (see Table 9).

Table 9: Types of tallies available in MCNP. The type of particle tallied is denoted by pl [9].

Mneumonic	Tally Type	particles *pl*	Fn Units	*Fn Units
F1:*pl*	surface current	N or P or N,P or E	#	MeV
F2:*pl*	average surface flux	N or P or N,P or E	#/cm^2	MeV/cm^2
F4:*pl*	average flux in a cell	N or P or N,P or E	#/cm^2	MeV/cm^2
FMESH4:*pl*	track-length tally over 3D mesh	N or P or E	#/cm^2	MeV/cm^2
F5a:*pl*	flux at a point or ring	N or P	#/cm^2	MeV/cm^2
FIP5:*pl*	pin-hole flux image	N or P	#/cm^2	MeV/cm^2
FIR5:*pl*	planar radiograph flux image	N or P	#/cm^2	MeV/cm^2
FIC5:*pl*	cylindrical radiograph flux image	N or P	#/cm^2	MeV/cm^2
F6:*pl*	energy deposition	N or P or N,P	MeV/g	jerks/g
F7:*pl*	fission energy deposition in a cell	N	MeV/g	jerks/g
F8:*pl*	pulse height distribution in a cell	P or E or P,E	pulses	MeV

5.2 Construction of OPF 430 pin diode by MCNP5

In This study, we used MCNP5 for modeling and simulating OPF 430 PIN diode. The Figure 55 shows the real structure and the design of OPF 430 that modeled by solid works program to simplify the identification of surfaces and cells (volumes) of real structure of P-N junction to build up the input files of MCNP5.

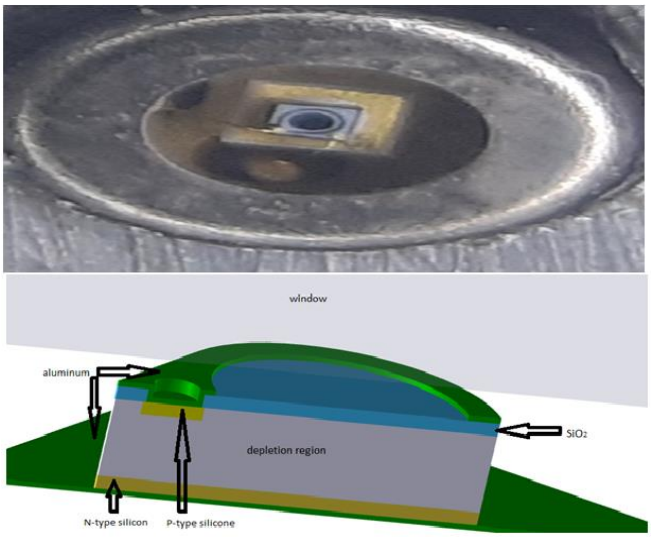


Figure 55: Modeling OPF430 pin diode by solid works (*Photo taken on site and modeled by solidworks***).**

The dimensions of OPF 430 diode are:

Window or glass is above appear in light gray color in a top with 1mm thick and 1mm^2

The aluminum appear as a green color act as P^+ with 0.2um width,

Air between glass and detector, which separated by 1cm,

$SIO_2$is in bleu appear in two-region take a role of N^+ doped silicon with 30um,

Silicon appear in grey act as a depletion region between yellow and blue has 300um,

The white color pointing to the vacuum outside the detector.

The detector is modeled by MCNP5 (see Figure 56).

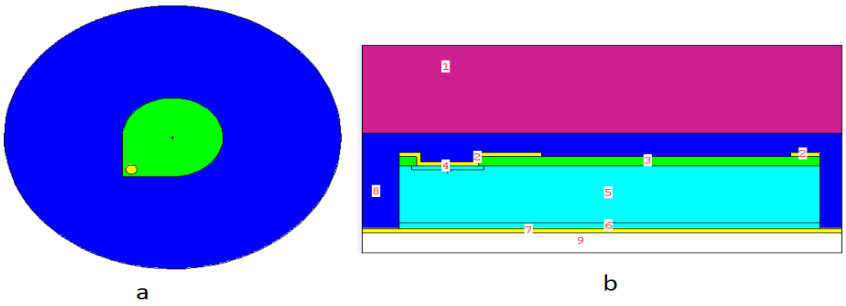


Figure 56: model OPF340 PIN diode in MCNP 5 where (a) is is the top of detector(x y) and (b) is side of the detector (x z) axis (*Photo taken on site and modeled by solidworks***).**

5.2.1 Penetration of radiation

Before discussing the characteristic of pin diode, we need first to simulate the attenuation of different radiation to guarantee the arrival of the interest radiation in the detector.

5.2.1.1 *Attenuation of x ray in glass*

The Table 10 obtained by MCNP5 shows the penetration of photon with different energy in paper:

Table 10: Efficiency of gamma rays

Energy (keV)	number
5	0,00E+00
10	1,50E-05
15	1,20E-03
20	3,60E-03
50	7,58E-03
500	8,03E-03
1000	8,05E-03

The curve in Figure 57 that obtained from the table above shows the penetration of photon with different energy in a window of the pin diode:

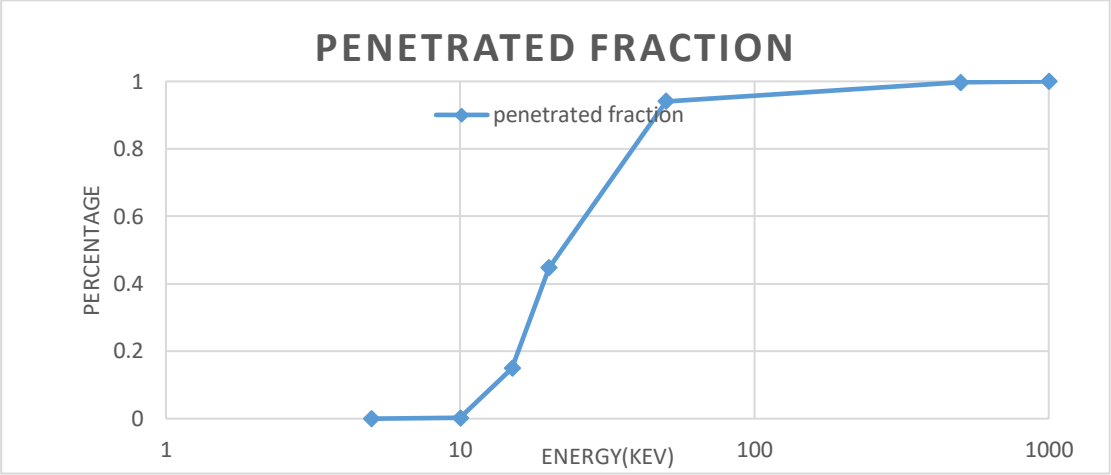


Figure 57: Penetration of gamma rays in the glass of the PIN diode.

The conclusion that obtained from this simulation is that, the number of photon penetrate the glass depends the energy of incoming photon. When the photon has energy ranged from zero to 10, keV there is no photon cross the glass, and if the photon has, energy raged from 11 keV to 25 keV, approximately 10 % from the photon cross the glass. The growth of number of photon penetrate the glass continue with the increase of energy until it reach probably 100% when the photon has energy equal 80 keV and above.

5.2.1.2 *Attenuation of x-ray in paper*

Obtained by MCNP5, Table 11 shows the penetration of photon with different energy in paper:

Table 11: Penetration of x-ray in paper.

Energy (keV)	Nombre of radiations crossing the paper
2	1,95E-03
5	1,61E-01
7	2,05E-01
10	2,25E-01
15	2,32E-01
20	2,34E-01
25	2,35E-01
35	2,35E-01
50	2,35E-01
70	2,35E-01
100	2,35E-01
120	2,35E-01
150	2,35E-01

The curve that obtained from the table above is in Figure 58.

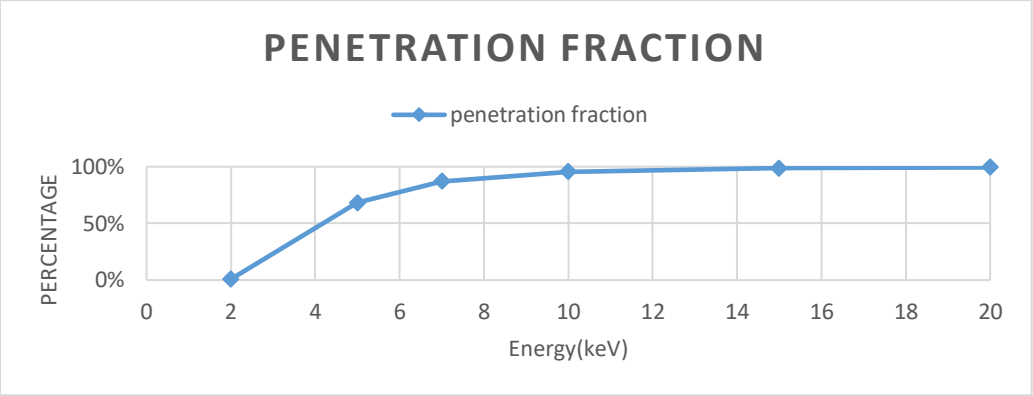


Figure 58: Penetration of gamma rays in the window of the PIN diode.

From this curved we can deduce that when the photon has energy equal 5% and above, then probably the majority of x rays become able to penetrate the paper.

5.2.1.3 *Attenuation of alpha particle in paper*

The picture below obtained by SRIM[15] Monte Carlo shows the path of alpha particle in paper of 4000A width:

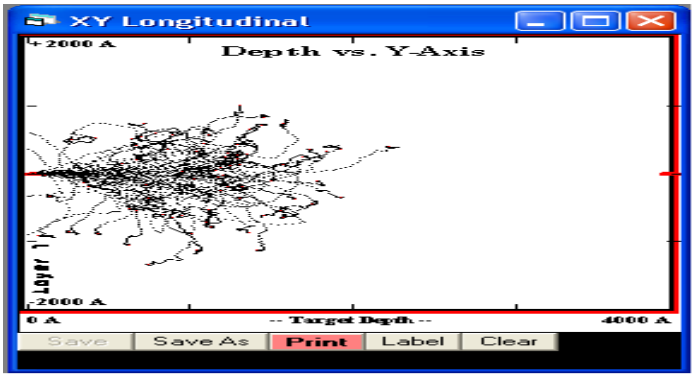


Figure 59: Path of alpha particles in the paper.

We can deduce from the picture that the alpha particle cannot penetrate the paper that has a width of 4000 A, so in our experience if we want to stop the alpha particle or just we were interesting X and gamma ray at low energy, then just we need to cover the source of Americium by the paper to guarantee the stooping of alpha particle.

Table 12 : Stopping power

Ion Energy	dE/dx Elec.	dE/dx Nuclear	Projected Range	Longitudinal Straggling	Lateral Straggling
10.00 keV	2.019E-01	3.838E-02	938 A	600 A	490 A
11.00 keV	2.119E-01	3.684E-02	1029 A	637 A	525 A
12.00 keV	2.216E-01	3.544E-02	1119 A	671 A	558 A
13.00 keV	2.315E-01	3.416E-02	1208 A	704 A	589 A

[15] James F. Ziegler, SRIM - The Stopping and Range of Ions in Matter, http://www.srim.org/

- **Nuclear stopping** is carried by a collision between two atoms, and can be described by classical kinematics. Nuclear stopping is elastic in nature and the energy lost by the incoming ion is transferred to the target atom, which is recoiled away from its lattice site. This process is responsible for the production of lattice disorder and most of the damage to the crystal structure of the target material.

- **Electronic stopping** is caused by interaction with the electrons of the target. Electronic stopping is inelastic in nature and the energy lost by incident ions is dissipated through the electron cloud into thermal vibrations of the target material[16].

- The relative importance of the two processes depends on the energy E and the atomic number Z of the ion. Note that nuclear collisions dominate at low energies and electronic collisions at high energies. For light ions electronic collisions will dominate where as for heavier ions nuclear collisions will dominate.

5.2.2 Efficiency of gamma rays

One of the most important result of our study by MCNP5 is to obtain the efficiency of OPF430 PIN diode of gamma ray detection with different energy, because gamma rays are experience a significant change in the experiment not like alpha particles, it is very necessary to the correctness of our study using this programs.

Table 13: Efficiency of gamma rays

Energy (keV)	Efficiency
1	0,00E+00
4	3,70E-02
5	1,99E-01
6	4,43E-01
7	6,76E-01
10	1,00E+00
15	6,69E-01
20	3,50E-01
30	1,11E-01
40	4,72E-02
50	2,23E-02
60	1,26E-02
70	7,63E-03
80	5,20E-03
90	3,75E-03
100	2,84E-03

The curve in Figure 60 that obtained from Table 13 is:

[16] http://www.jhaj.net/jasjeet/tcad/Learn3/l3d.htm

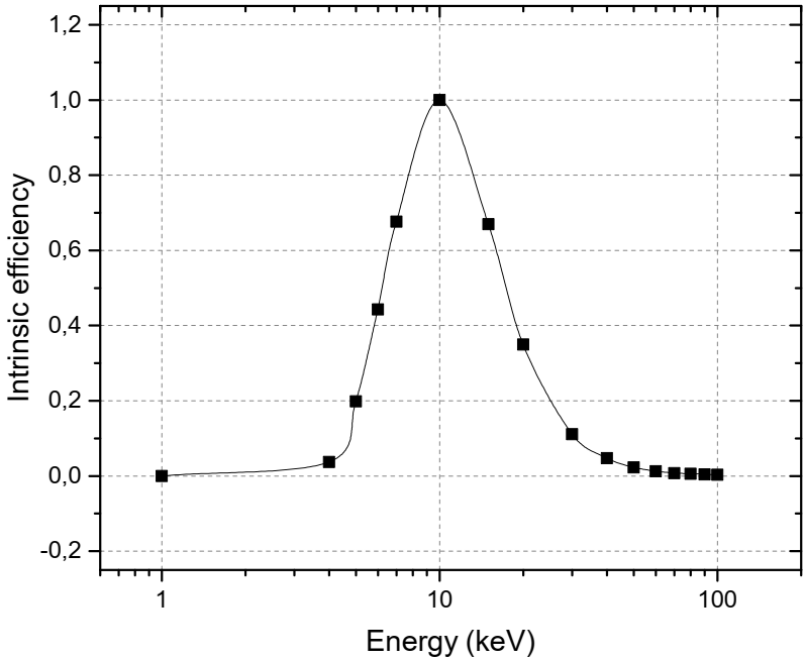


Figure 60: Simulate efficiency of gamma rays.

5.2.2.1 *Discussion*

The graph above shows the changes of detector efficiency depends the energy of incoming radiation In OPF 430 PIN diode.

At energy of gamma rays equal 10 keV the efficiency reach its maximum such the detector be able to capture all the incoming radiation. The efficiency dropped with the increasing of energy, at energy equal 100 keV the efficiency become 0%.

This result is very similar to the experimental data published in different papers [14].

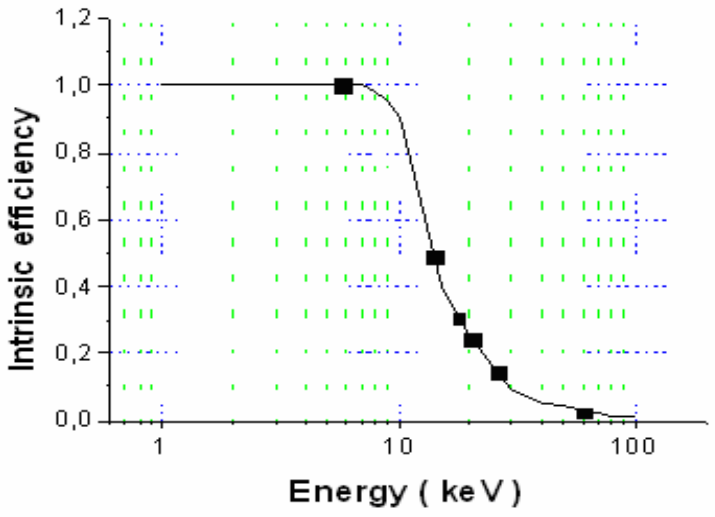


Figure 61: Simulate efficiency of gamma rays [14].

General Conclusion

In this work, we combined MCNP5 simulation and experiment to study the characteristic of OPF430 PIN diode. We focused on efficiency and resolution parameters to define the quality of this new detector. We also see the effect of the reverse bias on these parameters and compare our result to those found by the SSB detector. The results are as follows:

- OPF430 becomes an alternative instrument and a good choice for detecting X-ray, weak gamma and alpha particle. We got a good spectrum of alpha particles. We also obtained a weak X-ray spectrum due to the low capacity used in the preamplifier although the result was still satisfactory.
- OPF430 PIN diode has 100% efficiency for low energy gamma ray (~10 keV) while dropped into 0% at energy 100 keV .
- Good resolution obtained by OF 430 PIN diode, probably the same with SSB.
- 100% efficiency assumed for alpha particle obtained by OPF 430 PIN diode like SSB detector.
- The skew effect for the spectra is due to a charge multiplication that produced by the radiation such that there is no recombination of charges. we have the same observation for SSB but very clearly because of its great width of its active zone. this leads to confirming what we obtained by PIN diode.
- The rise time decreases when the reverse biased reference is increased due to the acceleration of the charges, which also leads to confirmation that the recombination of the charges becomes insignificant.
- The increasing of reverse biased improve the efficiency and resolution, on the other hand increase the dark current.
- We observed a spurious peak in the alpha and gamma ray spectrum, this may be due to the edge effect of the PIN diode, we need to take more data to understand where it is coming from.

We hope that researchers in this field will continue to explore and develop this detector to improve its sensitivity. However, they can add Peltier cooling or liquid nitrogen to reduce noise or minimize thermal excitation which will allow it to become more accurate for gamma and X-ray detection with other energy bands ranging to high-energy gamma rays.

Appendix:

MCNP Input for attenuation of photon in paper

```
c cell card  peper
  1    1 -0.76923 -11 12 -21
  2    2 -0.001205 -21 #1
  3    0        21

  11       pz 0
  12       pz -0.0104
  21       so 0.5

mode  p
m1    1000.          0.58364  $MAT
     6000.         0.374859 7000.         0.014531 8000.         0.018984
     9000.         0.005324 20000.        0.002662
m2    1000.         0.462423  $MAT
     6000.         0.323389 7000.         0.002773 8000.         0.208779
     12000.        0.000639 16000.        0.001211 19000.
0.000397
     20000.        0.000388
imp:p           1 1r                  0  $ 1, 3
sdef erg=150e-3 PAR=2 pos 0 0 0.3
nps 1e6
f1:p 12
```

References

[1] « Types of Ionizing Radiation ». https://www.mirion.com/learning-center/radiation-safety-basics/types-of-ionizing-radiation (consulté le 31 mai 2022).

[2] M. Oldham, « Radiation physics and applications in therapeutic medicine », *Phys. Educ.*, vol. 36, nº 6, p. 460-467, nov. 2001, doi: 10.1088/0031-9120/36/6/303.

[3] C. Mahuvava et F. C. P. Du Plessis, « Monte Carlo evaluation of the dose perturbation effect of hip prostheses for megavoltage photon radiotherapy », *Physica Medica*, vol. 31, p. S7, sept. 2015, doi: 10.1016/j.ejmp.2015.07.108.

[4] R. Roque, « X-ray imaging using 100 µm thick Gas Electron Multipliers operating in Kr-CO2 mixtures », 2018, doi: 10.13140/RG.2.2.16794.49600.

[5] Tindan, « The effect of neutron irradiation on the impedance of asbestos », CK Tedam University of Technology and Applied SciencesDepartment Science Education, 2008. [En ligne]. Disponible sur: https://www.academia.edu/1414204/The_effect_of_neutron_irradiation_on_the_impedance_of_asbestos

[6] G. F. Knoll, *Radiation detection and measurement*. New York: Wiley, 1979.

[7] P. Sigmund, *Particle penetration and radiation effects: general aspects and stopping of swift point charges*. Berlin ; New York: Springer, 2006.

[8] « PN Junction - Definition, Formation, Application, VI Characteristics and FAQs ». https://byjus.com/physics/p-n-junction/ (consulté le 1 juin 2022).

[9] R. Nave, « Semiconductor concepts: P-N Junction ». 2022. [En ligne]. Disponible sur: http://hyperphysics.phy-astr.gsu.edu/hbase/Solids/pnjun.html

[10] W. Wei-Chih, « Optical Detectors ». Department of Power Mechanical Engineering, National Tsing Hua University. [En ligne]. Disponible sur: https://depts.washington.edu/mictech/optics/me557/detector.pdf

[11] F. J. Ramírez-Jiménez, « X-Ray Spectroscopy with PIN diodes », in *AIP Conference Proceedings*, Morelia, Michoacan (Mexico), 2006, vol. 857, p. 121-133. doi: 10.1063/1.2359248.

[12] H. Spieler, *Semiconductor detector systems*. Oxford: Oxford university press, 2005.

[13] V. Radeka, « Low-Noise Techniques in Detectors », *Annu. Rev. Nucl. Part. Sci.*, vol. 38, nº 1, p. 217-277, déc. 1988, doi: 10.1146/annurev.ns.38.120188.001245.

[14] F. J. Ramírez-Jiménez, « X-Ray Spectroscopy with PIN diodes », in *AIP Conference Proceedings*, Morelia, Michoacan (Mexico), 2006, vol. 857, p. 121-133. doi: 10.1063/1.2359248.

[15] J. K. Shultis et R. E. Faw, « AN MCNP PRIMER », Dept. of Mechanical and Nuclear Engineering Kansas State University Manhattan, KS 66506, 2006. [En ligne]. Disponible sur: https://bl831.als.lbl.gov/~mcfuser/publications/MCNP/MCNP_primer.pdf